Available online at www.sciencedirect.com
SCIENCE DIRECT®
Journal of Asian Earth Sciences 23 (2004) 629–653
Journal of Asian Earth Sciences
www.elsevier.com/locate/jseaes

Sources of Phanerozoic granitoids in the transect Bayanhongor–Ulaan Baatar, Mongolia: geochemical and Nd isotopic evidence, and implications for Phanerozoic crustal growth

Bor-ming Jahn[a,*], Ramon Capdevila[a], Dunyi Liu[b], Antoine Vernon[a], G. Badarch[c]

[a]*Géosciences Rennes, Université de Rennes 1, 35042 Rennes Cedex, France*
[b]*Institute of Geology, Chinese Academy of Geological Sciences, 26 Baiwanzhuang Road, Beijing 100037, China*
[c]*Institute of Geology and Mineral Resources, Mongolian Academy of Sciences, Ulaanbaatar 210351, Mongolia*

Abstract

The Central Asian Orogenic Belt (CAOB) is renowned for massive generation of juvenile crust in the Phanerozoic. Mongolia is the heartland of the CAOB and it has been subject to numerous investigations, particularly in metallogenesis and tectonic evolution. We present new petrographic, geochemical and Sr–Nd isotopic analyses on Phanerozoic granitoids emplaced in west-central Mongolia. The data are used to delineate their source characteristics and to discuss implications for the Phanerozoic crustal growth in Central Asia. Our samples come from a transect from Bayanhongor to Ulaan Baatar, including three tectonic units: the Baydrag cratonic block (late Archean to middle Proterozoic), the Eo-Cambrian Bayanhongor ophiolite complex and the Hangay–Hentey Basin of controversial origin. The intrusive granitoids have ages ranging from ca. 540 to 120 Ma. The majority of the samples are slightly peraluminous and can be classified as granite (s.s.), including monzogranite, syenogranite and alkali feldspar granite. Most of the rocks have initial $^{87}Sr/^{86}Sr$ ratios between 0.705 and 0.707. Late Paleozoic to Mesozoic granitoids ($\leq$250 Ma) are characterized by near-zero $\varepsilon_{Nd}(T)$ values (0 to -2), whereas older granitoids show lower $\varepsilon_{Nd}(T)$ values (-1.5 to -7). The data confirm the earlier observation of Kovalenko et al. [Geochemistry International 34 (1996) 628] who showed that granitoids emplaced outside of the Pre-Riphean basement rocks are characterized by juvenile positive $\varepsilon_{Nd}(T)$ values, whereas those within the Pre-Riphean domain and the Baydrag cratonic block, as for the present case, show a significant effect of 'contamination' by Precambrian basement rocks. Nevertheless, mass balance calculation suggests that the granitoids were derived from sources composed of at least 80% juvenile mantle-derived component. Despite our small set of new data, the present study reinforces the general scenario of massive juvenile crust production in the CAOB with limited influence of old microcontinents in the genesis of Phanerozoic granitoids.

Keywords: Altaid Collage; Central Asia; Granitoids; Juvenile crust; Crustal growth; Nd isotopes; Phanerozoic granitoids

1. Introduction

Central Asia is a gigantic mosaic composed of a variety of terranes including Precambrian continental blocks, ancient island arcs, accretionary complexes, ophiolites and passive continental margins. These terranes were amalgamated in several periods from late Precambrian/early Paleozoic to late Mesozoic, and formed the world's largest Phanerozoic orogenic belts—the Central Asian Orogenic Belt (CAOB). The CAOB, bounded by the Siberian and North China cratons, represents a complex evolution of orogenic belts and it has also been termed Altaid Tectonic Collage by Sengör and his associates (Sengör et al., 1993; Sengör and Natal'in, 1996). According to them, it was formed by successive accretion of arc complexes, accompanied by emplacement of voluminous subduction zone granitic magmas. In addition, they consider the general absence of nappe complexes imbricating older continental crust as a characteristic feature of the Altaid Collage. It is the voluminous granitic intrusions, mostly of juvenile character, that distinguish the CAOB from other classical Phanerozoic orogenic belts (Kovalenko et al., 1996; Jahn et al., 2000a,b; Wu et al., 2000, 2002; Jahn, 2003).

In this paper we report new chemical and Sr–Nd isotopic compositions of Phanerozoic granitoids emplaced in central Mongolia. Our sampling sites followed the excursion route during the IGCP-420 second workshop in 1999, traversing from west of Bayonhongor to Ulaanbaatar. According to

* Corresponding author. Address: Department of Geoscience, National Taiwan University, P.O. Box 13-318, Taipei 106, Taiwan. Tel.: +886-2-2363-0231/2378; fax: +886-2-2363-6095.
E-mail address: jahn@ccms.ntu.edu.tw (B.-m. Jahn).

1367-9120/03/$ - see front matter © 2003 Elsevier Ltd. All rights reserved.
doi:10.1016/S1367-9120(03)00125-1

the new terrane map of Badarch et al. (2002), our granitoid samples come from a variety of terranes, including a late Archean to early Proterozoic cratonic block (Baydrag), a Neoproterozoic or Eocambrian ophiolite (Bayanhongor), a passive continental margin, a Devonian to Carboniferous turbidite basin (Hangay–Hentey Basin), and a Permo-Triassic Hangay batholith. Some of them were emplaced within an ancient cratonic block, hence their petrogenesis could have involved contamination or participation of old crustal rocks. Due to the fact that our sampling was not done in a systematic way and the samples do not belong to the same magmatic suite, a detailed discussion of petrogenetic processes is not possible. Instead, this paper underlines the following two points: (1) characterization of the Phanerozoic granitoids and tracing their sources using geochemical and Nd–Sr isotopic techniques, and (2) discussion on the Phanerozoic crustal growth in the CAOB in light of the available data for Mongolia and adjacent areas.

2. Lithological characters and emplacement periods of granites in the CAOB

According to Kovalenko et al. (1995), igneous activity in Mongolia and Transbaikalia continued throughout the entire Phanerozoic without significant interruption. Since the early Paleozoic numerous granitic rocks have been emplaced. They include (1) the calc–alkaline series (tonalite–granodiorite–granite) of 'Caledonian' ages in northern Mongolia and Transbaikalia (e.g. Angara-Vitim batholith, Litvinovsky et al., 1994); (2) the 'late Caledonian' calc–alkaline series in western Mongolia and the alkaline series in Tuva, Sayan, Mongolian Altai, and vast areas in northern Mongolia and Transbaikalia; (3) the 'Hercynian' (late Carboniferous to Permian) alkaline series in southern Mongolia and in northern Mongolia to Transbaikalia; Late Permian granitoids of the calc–alkaline series, represented by the vast Hangay batholith ($\approx$100,000 km^2) in west-central Mongolia, and the granitic intrusions in the Gorny Altai region (Vladimirov et al., 1997); and (4) the early Mesozoic ($\approx$200 Ma) granites of the calc–alkaline series and S-type granites in the southern Altai and the Mongol–Okhotsk belt, plus the alkaline to peralkaline series in Transbaikalia. The lithologic types are composed mainly of alkaline and peralkaline granites, syenogranites, syenites and minor granodiorites. Many plutons contain abundant miarolitic cavities and igneous layering formed by biotite-rich bands. Mafic enclaves are generally rare; but in Transbaikalia significant amounts of mafic rocks occur as enclaves and syn-plutonic dykes in granitoids of various ages (Zanvilevich et al., 1995; Wickham et al., 1995, 1996).

The ages of granites roughly decrease from north to south within the CAOB. In Transbaikalia and northern Mongolia, five main stages of K-rich magmatic activity have been distinguished (Zanvilevich et al., 1995; Wickham et al., 1995, 1996): (1) Ordovician–Silurian ($\approx$450 Ma), (2) Devonian ($\approx$375 Ma), (3) Early Permian ($\approx$280 Ma), (4) Late Permian ($\approx$250 Ma), and (5) Triassic ($\approx$220 Ma). In northern Xinjiang, granitic plutons that intrude into the Altai orogen and Junggar Terrane are mainly syn-orogenic granitoids, with minor post-orogenic A-type granites. These granitoids were mainly emplaced in two periods: late Caledonian (377–408 Ma) and Hercynain (290–344 Ma; Zou et al., 1988; Liu, 1990). The Keketuohai pluton was recently dated at 387 $\pm$ 6 Ma (SHRIMP zircon U–Pb; S. Wilde, pers. comm.).

Widespread granitic rocks are exposed in NE China, the easternmost part of the CAOB. Emplacement of granitic intrusions took place in two main periods (Wu et al., 2002): (1) in late Paleozoic (290–260 Ma), represented by the calc–alkaline suites in the Jiamusi Block and A-type granites in the Xing'an Block) and (2) in Mesozoic (200–120 Ma), also by both calc–alkaline and A-type granites. The A-type granites were probably formed in association with post-collisional slab break-off (for Permian granites), lithospheric delamination (Triassic–Jurassic), and anorogenic rifting initiated by Paleo-Pacific subduction (Cretaceous; Wu et al., 2002).

According to Sengör et al. (1993), Central Asia grew by successive accretion of subduction complexes along a single magmatic arc now found contorted between Siberia and Baltica. They recognized the main difference between the Altaids (= CAOB) and other type collisional orogens such as the Alps and the Himalayas in that the Altaids show a paucity of extensive ancient gneiss terrains or Precambrian microcontinents. Moreover, no Alpine- or Himalayan-type crystalline nappe complexes imbricating pre-existing continental crust were recognized within the Altaid collage, and that high-K granites were considered to be produced by anatexis, and only became abundant in the Permian. The above hypothesis on tectonic evolution and structural analyses has been a point of controversy in the last few years. Nevertheless, the overall scheme for the growth of Central Asia by lateral accretion of subduction complexes is probably correct except that the role of ancient microcontinents has been much underestimated, and the vertical accretion via basaltic underplating has not been considered.

In view of certain problems encountered in the tectonic model of Sengor and his associates (Sengör et al., 1993; Sengör and Natal'in, 1996), Badarch et al. (2002) presented an alternative view of tectonic evolution of Mongolia using the concept of terrane analysis. They distinguished 44 terranes and classified them into cratonic, metamorphic, passive margin, island arc, forearc/backarc, accretionary complex, and ophiolite types. They also provided stratigraphic columns for all terranes. In their analysis, the Precambrian cratonic blocks in the Hangay region acted as a central nucleus around which Paleozoic arcs, backarc/forearc basin assemblages, associated subduction complexes and continental slivers were accreted. They noticed that the temporal and spatial order of accretion was complex and not simply from north to south with time.

3. Geology of the sampling terranes

Our samples came mainly from a northeastward traverse from the Baydrag microcontinent, the Bayanhongor ophiolite, the Dzag terrane and the Hangay–Hentey Basin where Ulaanbaatar is situated (Fig. 1). The precise localities are given in Table 2, instead of Table 1, for the reason of a better space arrangement. According to Badarch et al. (2002), the Baydrag terrane is composed of two metamorphic complexes: (1) the Baydrag complex, made up of late Archean tonalitic gneiss, granulite, amphibolites, and minor quartzite (Mitrofanov et al., 1985); the tonalitic gneiss has recently

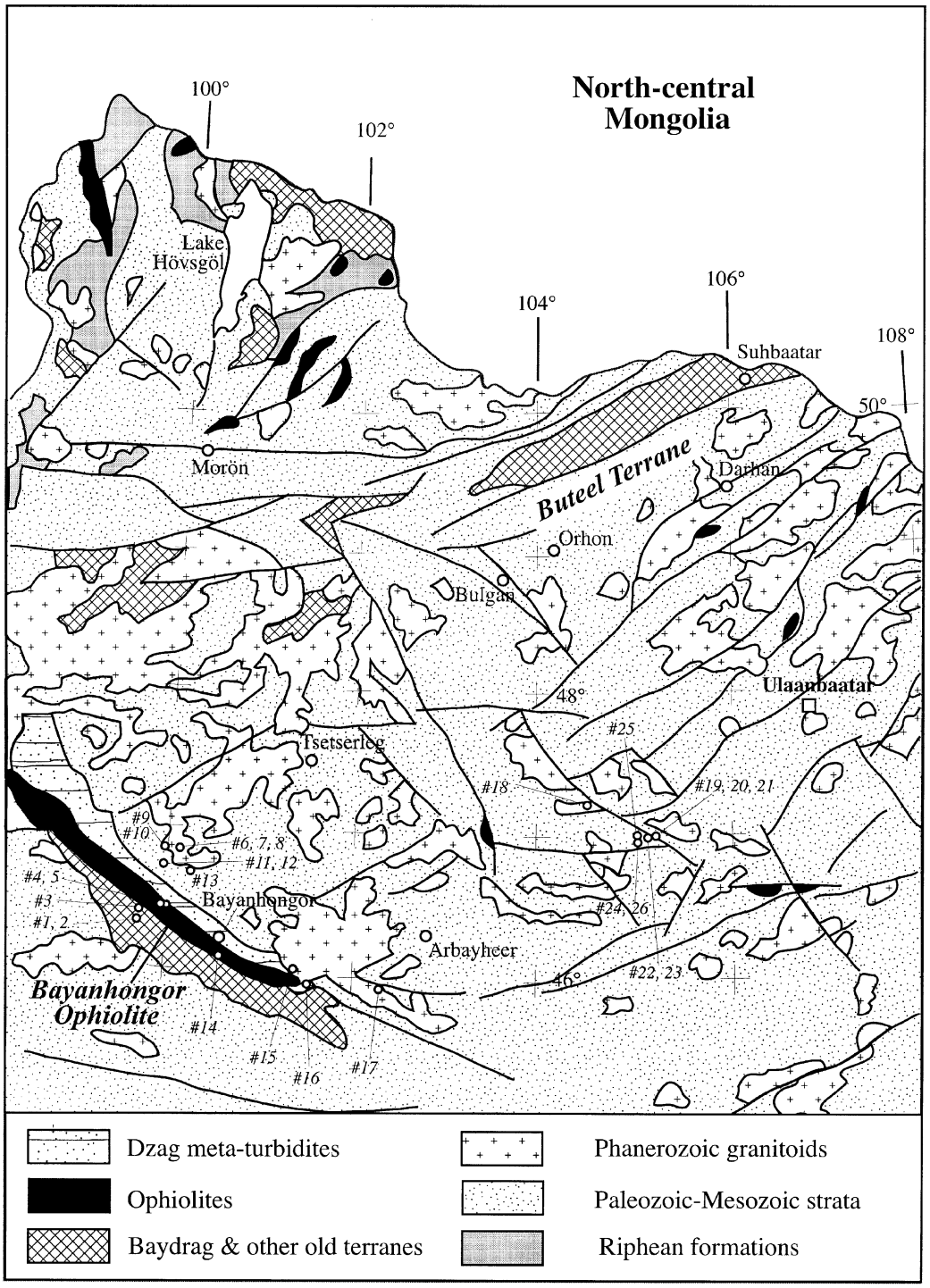

Fig. 1. Geological sketch map of north-central part of Mongolia and the sampling localities with sample numbers. Note that the prefix of sample number is dropped, thus CF99-01 is designated as #1, and so on. Map source: Geotectonic Map of Mongolia (1/2,500,000), 1998, D. Dorjnamjaa (chief editor), Mongolian Academy of Sciences, Ulaanbaatar.

Table 1
Chemical compositions of Mongolian Granitoid rocks

Sample no.	M99-01	M99-02	M99-03	M99-04	M99-05	M99-06	M99-07	M99-08	M99-09	M99-10	M99-11	M99-12
Rock type	Granite	Granite	Granodiorite	Diorite	Monzogranite	Granite	Granite	Granite	Granite	Granitic dike	Meta-pelite	Meta-pelitic ss
Major elements (in %; blank represents lower than the detection limit)												
SiO_2	70.87	71.17	66.5	53.16	67.98	71.95	66.07	71.57	67.3	74.71	57.14	63.77
Al_2O_3	16.01	15.65	16.24	17.31	15.93	14.9	16.12	15.05	15.83	13.97	17.72	11.85
Fe_2O_3	1.87	1.7	4.11	8.25	3.19	1.65	3.95	1.73	3.57	0.88	7.34	5.43
MnO	0.04	0.04	0.04	0.13	0.04		0.05		0.04	0.03	0.03	0.07
MgO	0.43	0.43	1.12	5.58	0.97	0.43	1.36	0.43	1.07		3.87	3.47
CaO	2.28	1.6	3.17	7.54	2.46	1.59	3.02	1.34	2.98	0.96	2.22	4.5
Na_2O	4.01	4.31	4.04	3.8	3.83	3.96	4.02	3.9	3.69	3.84	2.11	2.59
K_2O	3.24	3.63	3.38	1.14	3.9	4.59	3.78	4.7	3.97	4.87	2.99	1.1
TiO_2	0.18	0.16	0.6	0.88	0.37	0.25	0.6	0.26	0.54		0.76	0.64
P_2O5	0.09	0.07	0.2	0.31	0.14	0.07	0.2	0.11	0.19		0.19	0.17
LOI	1.02	1.26	0.6	1.85	1.11	0.46	0.74	0.75	0.76	0.38	5.51	6.23
Total	100.04	100.02	100.00	99.95	99.92	99.85	99.91	99.84	99.94	99.64	99.88	99.82
Trace elements (in ppm; blank represents lower than the detection limit)												
Cs	1.98	2.07	0.61	3.42	3.36	11.6	15.1	15.8	13.8	9.70	5.43	2.64
Rb	93.0	102	74.4	32.1	115	203	159	171	124	251	110	41.1
Sr	1069	843.5	680.6	854.0	479.0	215.4	421.9	202.5	470.5	72.6	132.8	191.4
Ba	1724	1577	1342	621.0	1022	612.8	813.3	614.3	1314	168.7	676.1	297.6
Be	2.44	1.98	1.47	1.76	2.96	4.46	9.67	4.34	4.58	4.56	2.18	1.00
Nb	7.05	6.91	12.80	5.02	7.39	9.93	9.68	8.87	8.21	16.99	10.45	9.02
Ta	0.65	0.71	1.40	0.41	0.93	1.64	1.12	1.42	1.08	1.81	0.89	0.77
Th	6.20	6.57	5.79	3.40	16.32	34.31	19.56	30.56	11.28	17.21	11.52	8.54
U	0.87	0.96	0.47	0.89	2.77	9.57	3.75	5.70	3.58	5.32	2.65	2.00
Pb	30.8	29.6	16.3	11.4	22.6	40.0	23.4	35.2	23.1	76.8	16.0	7.6
Zr	124	103	242	86	155	151	192	126	164	60	178	148
Hf	3.4	2.9	5.6	2.3	4.7	4.8	5.1	3.8	4.7	2.8	4.8	4.2
Y	8.49	9.71	16.73	13.47	7.57	4.94	10.50	4.24	8.20	10.27	28.56	23.53
V	14.2	11.4	49.4	161.5	28.6	15.5	48.0	13.2	34.5		155.7	85.2
Co	1.6	1.3	6.6	26.3	5.0	2.3	7.2	2.1	5.9	0.3	17.5	8.2
Ni				57.2	5.1		7.9		6.1		57.8	31.6
Cr	11.1	20.8	12.6	198.2	19.7	35.7	28.2	8.9	21.4	21.0	117.8	68.8
W	0.58	0.34	0.11	0.59	0.86	3.60	32.42	0.45	1.83	0.20	1.67	1.55
Cu				43.6		6.7	6.5	7.8			51.0	23.3
Zn	60.0	32.7	59.0	94.6	49.1	45.9	71.6	36.6	63.7	34.2	131.6	81.3
Ga	22.7	19.7	19.7	22.0	18.8	22.6	23.5	19.3	21.1	26.7	26.1	15.1
Ge	1.8	1.5	1.1	1.3	1.1	1.2	1.4	1.3	1.1	1.9	2.1	1.7
Sn	2.2	1.9	2.1	0.9	1.2	4.0	17.1	4.3	5.7	7.8	3.1	2.1
As	0.8	0.7	2.8	3.8	3.6						26.0	15.5
K/Rb	289	296	377	295	282	188	198	229	265	161	226	222
Rb/Sr	0.09	0.12	0.11	0.04	0.24	0.94	0.38	0.84	0.26	3.45	0.83	0.21
K/Ba	15.6	19.1	20.9	15.2	31.7	62.2	38.6	63.5	25.1	239.6	36.7	30.7
Nb/Ta	10.8	9.8	9.1	12.4	8.0	6.1	8.7	6.2	7.6	9.4	11.7	11.7
Zr/Hf	36.3	35.7	43.4	37.6	33.1	31.5	37.3	33.5	34.8	21.5	36.8	35.5
Y/Ho	31.5	30.1	27.1	26.4	28.0	28.4	33.2	28.8	30.4	35.4	28.2	27.8
La/Nb	3.79	3.55	4.11	5.31	4.13	3.29	3.71	3.50	3.71	0.44	3.26	3.17
La/Ta	41.1	34.8	37.4	65.8	32.9	19.9	32.2	21.9	28.1	4.2	38.1	37.2
La/Th	4.31	3.74	9.08	7.82	1.87	0.95	1.84	1.02	2.70	0.44	2.95	3.35
Th/U	7.1	6.8	12.4	3.8	5.9	3.6	5.2	5.4	3.1	3.2	4.4	4.3

La	26.71	24.55	52.57	26.63	30.55	32.64	35.94	31.09	30.48	7.54	34.03	28.60
Ce	51.71	47.23	102.66	54.26	58.23	66.25	68.93	61.62	57.01	15.59	69.62	58.27
Pr	5.57	5.23	10.99	6.48	6.27	6.43	7.44	6.07	6.06	1.70	8.22	6.92
Nd	19.23	18.92	36.62	25.56	22.41	21.17	27.02	19.62	22.64	6.87	31.34	27.95
Sm	3.25	3.40	6.15	5.15	3.57	3.60	4.87	3.17	3.95	1.74	5.37	5.53
Eu	0.86	0.74	1.30	1.53	0.96	0.65	1.15	0.60	1.30	0.29	1.32	1.36
Gd	2.28	2.42	4.04	3.79	2.28	2.00	3.48	1.92	3.02	1.83	5.11	4.85
Tb	0.32	0.33	0.62	0.47	0.31	0.28	0.45	0.27	0.36	0.26	0.77	0.68
Dy	1.67	1.80	3.27	2.71	1.64	1.31	2.17	1.02	1.82	1.55	4.65	4.18
Ho	0.27	0.32	0.62	0.51	0.27	0.17	0.32	0.15	0.27	0.29	1.01	0.85
Er	0.75	0.94	1.66	1.35	0.69	0.43	0.95	0.37	0.71	0.90	3.15	2.51
Tm	0.11	0.14	0.23	0.19	0.11	0.05	0.13	0.05	0.10	0.14	0.49	0.41
Yb	0.69	0.92	1.46	1.08	0.61	0.35	0.75	0.33	0.54	0.90	3.49	2.76
Lu	0.12	0.16	0.23	0.19	0.10	0.06	0.13	0.05	0.07	0.13	0.50	0.36
Eu/Eu*	0.98	0.80	0.81	1.07	1.05	0.75	0.86	0.75	1.17	0.50	0.78	0.81
Sample no.	M99-13	M99-14	M99-15	M99-16	M99-17	M99-18	M99-19	M99-20	M99-21	M99-24	M99-25	M99-26
Rock type	Micro-granite	Anorthosite	Granite	Granite	Grano-diorite	Granite	Ongonite	Ongonite	Ongonite	Aplite	Granite	Granite
Major elements (in %; blank represents lower than the detection limit)												
SiO_2	72.6	44.95	73.99	70.79	65.02	70.38	71.24	72.92	71.67	75.21	73.98	73.52
Al_2O_3	14.05	27.49	13.85	14.38	16.44	15.29	17.13	16.43	17.32	13.69	13.76	13.74
Fe_2O_3	3	1.71	0.99	2.44	4.12	2.37	0.26	0.17	0.26	0.52	1.52	1.99
MnO	0.06	0.03		0.03	0.04	0.05	0.15	0.23	0.15	0.2	0.03	0.06
MgO	0.69	3.54	0.2	0.6	1.43	0.77					0.25	0.38
CaO	1.21	15.71	1.19	1.1	3.81	2.49	0.43	0.12	0.13	0.43	0.9	1.21
Na_2O	4.51	2.85	3.33	3.76	3.9	3.83	5.69	5.34	5.71	4.71	3.72	3.59
K_2O	3.02	0.06	5.36	5.04	3.22	3.55	3.37	3.35	3.19	4.46	4.99	4.85
TiO_2	0.42	0.07	0.1	0.45	0.63	0.37					0.2	0.27
P_2O5	0.12		0.05	0.16	0.19	0.13					0.06	0.1
LOI	0.69	3.36	0.74	1.12	1.11	0.6	1.44	1.54	1.26	0.43	0.41	0.51
Total	100.37	99.77	99.80	99.87	99.91	99.83	99.71	100.10	99.69	99.65	99.82	100.22
Trace elements (in ppm; blank represents lower than the detection limit)												
Cs	2.89		2.04	2.99	2.34	5.60	67.7	102.8	88.0	25.9	7.14	12.4
Rb	82.3	2.3	217	236	98.8	167	2074	2773	2271	588	214	261
Sr	201.4	266.2	206.1	297.0	508.4	248.5	9.4	14.0	24.5	6.1	207.4	167.6
Ba	619.7	54.2	416.4	630.8	822.6	430.7	5.8	9.7	10.7	6.1	432.6	464.7
Be	2.68		3.39	4.63	1.31	3.77	46.13	15.01	14.21	7.66	6.32	6.00
Nb	10.28		3.72	16.92	7.84	12.39	68.81	45.18	55.60	56.04	11.28	19.66
Ta	0.92		0.35	2.69	0.61	1.68	112.97	93.03	76.09	5.43	1.74	2.76
Th	10.43		69.29	54.21	9.96	19.06	16.81	12.09	15.52	32.05	59.42	44.55
U	2.53		4.65	4.55	1.24	1.51	13.94	12.23	5.37	9.15	6.37	6.67
Pb	20.9		43.2	39.6	21.9	24.4	123.7	49.1	72.3	161.4	59.5	39.7
Zr	293	2	140	269	184	176	45	14	35	98	170	197
Hf	7.6	0.0	4.4	7.7	5.1	5.3	12.4	5.8	9.3	9.4	5.7	5.4
Y	32.61	1.86	3.79	23.69	7.64	17.20	22.07	8.57	16.87	9.62	12.80	27.11
V	35.7	46.9	7.5	21.7	52.6	25.5					7.8	13.9
Co	3.2	13.0	1.1	3.1	8.2	3.6					1.1	1.9
Ni		88.5			8.5							
Cr	18.1	230.2	18.6	14.4	28.9	12.7	9.6	14.4	17.3	13.7	7.4	7.7
W	0.91	1.11		0.38	0.31	0.23	7.22	6.52	5.01	2.16	0.51	0.30
Cu		10.9			5.8	7.2						
Zn	73.0	12.2	27.4	59.8	75.8	52.6	101.3	71.5	34.4	33.3	51.3	46.5

(*continued on next page*)

Table 1(*continued*)

Sample no.	M99-13	M99-14	M99-15	M99-16	M99-17	M99-18	M99-19	M99-20	M99-21	M99-24	M99-25	M99-26
Rock type	Micro-granite	Anor-thosite	Granite	Granite	Grano-diorite	Granite	Ongonite	Ongonite	Ongonite	Aplite	Granite	Granite
Ga	20.6	13.8	20.3	21.5	22.6	20.8	59.3	70.5	64.3	38.1	23.0	21.7
Ge	1.6	1.1	1.2	1.2	1.1	1.5	9.9	10.2	9.5	3.5	1.3	1.8
Sn	2.8		2.3	10.4	1.5	5.0	44.8	42.0	33.7	11.4	4.3	7.5
As	2.6			0.5	2.9		2.8	1.8	1.6	0.8	2.2	0.9
K/Rb	305	212	205	177	271	177	13	10	12	63	193	154
Rb/Sr	0.41	0.01	1.05	0.80	0.19	0.67	220.8	197.6	92.6	96.1	1.03	1.56
K/Ba	40.4	9.2	106.8	66.3	32.5	68.4	4862	2863	2470	6076	95.7	86.6
Nb/Ta	11.2		10.6	6.3	12.9	7.4	0.6	0.5	0.7	10.3	6.5	7.1
Zr/Hf	38.4	42.7	31.6	35.2	36.2	33.2	3.6	2.3	3.8	10.4	29.7	36.6
Y/Ho	28.9	23.5	26.2	30.8	29.0	27.9	34.1	23.0	32.3	43.2	31.0	32.9
La/Nb	3.30		11.14	3.29	4.00	2.96	0.11	0.09	0.13	0.10	5.46	2.55
La/Ta	36.9		118.7	20.8	51.7	21.8	0.07	0.04	0.10	1.03	35.4	18.1
La/Th	3.26		0.60	1.03	3.15	1.92	0.46	0.34	0.47	0.17	1.04	1.12
Th/U	4.1		14.9	11.9	8.0	12.7	1.2	1.0	2.9	3.5	9.3	6.7
La	33.96	0.54	41.42	55.75	31.36	36.69	7.73	4.11	7.33	5.58	61.65	50.05
Ce	73.30	1.02	81.92	133.27	60.16	72.11	29.08	19.55	24.86	11.59	112.38	102.06
Pr	8.30	0.17	8.49	13.73	6.54	8.13	4.23	2.82	4.04	1.18	10.82	10.95
Nd	32.89	0.83	28.43	49.83	24.90	29.96	14.52	8.16	13.27	3.59	33.49	37.20
Sm	6.10	0.25	4.12	8.99	4.34	5.32	6.38	3.80	5.67	0.72	5.12	6.78
Eu	1.07	0.30	0.50	1.00	1.07	0.69	0.01	0.01	0.05	0.05	0.66	0.90
Gd	5.75	0.28	1.85	6.25	3.07	4.44	4.19	1.78	3.43	0.63	2.94	5.56
Tb	0.90	0.04	0.23	0.84	0.37	0.65	0.74	0.45	0.68	0.12	0.51	0.76
Dy	5.38	0.37	0.94	4.69	1.76	3.39	4.13	2.62	3.52	0.83	2.52	4.56
Ho	1.13	z0.08	0.14	0.77	0.26	0.62	0.65	0.37	0.52	0.22	0.41	0.82
Er	3.36	0.20	0.46	2.14	0.69	1.69	1.71	1.02	1.22	0.86	1.28	2.27
Tm	0.56	0.03	0.05	0.30	0.09	0.21	0.28	0.20	0.23	0.21	0.21	0.40
Yb	4.01	0.17	0.41	1.88	0.67	1.33	2.37	1.78	1.78	2.11	1.55	2.84
Lu	0.62	0.02	0.05	0.28	0.10	0.20	0.34	0.22	0.24	0.43	0.25	0.43
Eu/Eu*	0.56	3.47	0.57	0.41	0.91	0.44	0.01	0.01	0.03	0.23	0.53	0.46

been dated by SHRIMP analysis at 2833 ± 35 Ma (Kozakov et al., 2001); and (2) the Bumbuger complex, comprising schist, gneiss, marble, quartzite and charnockite, intruded by granite and granodiorite dikes of 2.36 and 1.85 Ga (Kotov et al., 1995). The basement gneisses are overlain unconformably by sandstone, quartzite, and dolomite of probable Neoproterozoic age (K–Ar muscovite age of ca. 700 Ma; Teraoka et al., 1996). The Baydrag terrane has been subjected to several episodes of granitoid intrusion, including TTG intrusions in the basement rocks in the early Proterozoic (2.4–1.8 Ga), Ordovician granitic intrusions (≈470 Ma, Oyungerel and Takahashi, 1999) and Permian alkaline granite intrusions (≈250–280 Ma). This terrane has been interpreted as a microcontinental block (Mitrofanov et al., 1985; Kozakov et al., 1997).

The Bayanhongor ophiolite terrane forms a NW–SE-striking zone about 300 km long and up to 20 km wide. The ophiolite is the largest in Mongolia and possibly the entire Central Asia. It is exposed continuously from near the town of Dzag to the city of Bayanhongor. A detailed lithological and structural study of the terrane is published by Buchan et al. (2001). A complete ophiolite stratigraphy, including ultramafic cumulates, gabbro, anorthosite, sheeted dikes, pillow lava, chert and limestone, is observed. However, the ophiolite sequence is dismembered into blocks, which are enclosed in a matrix of sheared, serpentinized ultramafic rocks. A gabbro has been dated at 569 ± 21 Ma by the Sm–Nd mineral isochron method (Kepezhinskas et al., 1991), which reflects the time of ophiolite formation. The timing of the ophiolite emplacement (obduction) was constrained at ca. 540 Ma by zircon U–Pb age determination for granite plutons and dikes that intrude the ophiolite (Buchan et al., 2002).

The Dzag terrane (or Dzag series), located to the NE of the Bayanhongor ophiolite, is composed of highly deformed pelitic and psammitic chlorite–mica schists of lower greenschist facies. Less metamorphosed, fine-grained interbedded siltstone, sandstone and shale contain rounded quartz grains and preserve sedimentary structures that resemble a turbidite sequence (Buchan et al., 2001). Kurimoto and Tungalag (1998) obtained two white-mica K–Ar dates of 454 ± 9 and 445 ± 9 Ma. They interpreted these dates to be the time of an Ordovician regional metamorphism. The Dzag schists are dominated by a well-developed SW-dipping shear fabric, NE-vergent asymmetric folds, and NE-directed overthrusts. The terrane is tectonically overlain by the Bayanhongor ophiolite and underlain by Devonian–Carboniferous Hangay–Hentey sediments, and is intruded by Ordovician (?), Carboniferous and Permian granites (Badarch et al., 2002).

The Hangay–Hentey Basin occupies a large area in central to north-central Mongolia. The basin is filled with Cambrian to Carboniferous sediments, mainly of shallow marine origin, and volcanic rocks. It is intruded by an impressive amount of early Paleozoic to Mesozoic granitoids, forming the Hangay and Hentey plateaux. The granitoid belt extends to Transbaikalia and further to the Sea of Okhotsk. The belt forms the largest granitoid province in the CAOB and the entire Asia. The tectonic significance of the basin is controversial. Zorin (1999) and Parfenov et al. (1999) consider the basin as an accretionary wedge, whereas Sengör and Natal'in (1996), following Zonenshain et al. (1990), regard it as part of the Mongol–Okhotsk oceanic gulf. Alternatively, it has also been suggested to be a back-arc basin formed within an Andean-type margin produced by northward subduction of the South Mongolian oceanic plate (Gordienko, 1987), or as a post-orogenic successor basin formed on early Paleozoic basement of northern Mongolia (Ruzhentsev and Mossakovskiy, 1996). Note that although the Mongol–Okhotsk ocean basin has been frequently hypothesized in tectonic models, its closure history and the location of its suture zone have never been clearly defined (Badarch et al., 2002).

Structural, lithological and geochemical analyses suggest that the Bayanhongor ophiolite formed in a spreading centre within an ocean basin (Kepezhinskas et al., 1991; Buchan et al., 2001), and was later obducted onto the Dzag passive margin terrane and itself overthrust by the Baydrag cratonic block. The Bayanhongor ophiolite marks a collisional suture zone between the Baydrag and Hangay Precambrian blocks (Buchan et al., 2001).

4. Analytical procedures

Chemical compositions were measured by ICP-AES (major elements) and ICP-MS (trace elements) at the Analytical Center of the CRPG at Nancy (France). Analytical uncertainties are ± 1 to 10% for major elements depending on the concentration level; and ± 5 to 15% for trace elements, also depending on concentration level. For REE abundances, the uncertainty is estimated at ± 5%.

Rb–Sr and Sm–Nd isotopic analyses were performed in the geochemical laboratory of Géosciences Rennes. The analytical procedures for Sr–Nd isotopic analyses are the same as reported earlier (Jahn et al., 1996, 1999). Analytical precisions, Sr–Nd isotope standard and normalization values, and blank levels can be found in the footnotes of Table 2. The decay constants used in age computation are $^{87}Rb = 0.0142\ Ga^{-1}$ and $^{147}Sm = 0.00654\ Ga^{-1}$. Sm–Nd model ages are calculated in two ways. The one-stage model age ($T_{DM} - 1$) is calculated assuming a linear Nd isotopic growth of the depleted mantle reservoir from $\varepsilon_{Nd} = 0$ at 4.56 Ga to $\varepsilon_{Nd} = +10$ at the present.

$$T_{DM}(1) = 1/\lambda \ln\{1 + [(^{143}Nd/^{144}Nd)s - 0.51315]/[(^{147}Sm/^{144}Nd)s - 0.2137]\},$$

where s = sample, λ = decay constant of ^{147}Sm ($0.00654\ Ga^{-1}$).

Table 2
Sr–Nd isotope data of the rocks from Mongolia

Sample no.	Rock type	Locality	Coordinates		Age (Ma) estim.	Rb (ppm)	Sr (ppm)	$^{87}Rb/^{86}Sr$	$^{87}Sr/^{86}Sr$	$2\sigma_m$	I_{Sr}	Sm (ppm)	Nd (ppm)	$^{147}Sm/^{144}Nd$	$^{143}Nd/^{144}Nd$	$2\sigma_m$	εNd(0)	εNd(T)	$f_{Sm/Nd}$	T_{DM1} (Ma)	T_{DM2} (Ma)
			N	E																	
M99-01	Granite	Tsagaan Nuruu	46°21.81′	99°44.36′	514	99.7	1063	0.271	0.709717	7	0.7077	3.09	18.45	0.1012	0.511952	3	−13.4	−7.1	−0.49	1619	1894
M99-02	Granite	Tsagaan Nuruu	46°22.29′	99°45.99′	514	113.4	920.4	0.356	0.710454	7	0.7078	3.37	19.42	0.1049	0.511988	7	−12.7	−6.7	−0.47	1624	1841
M99-03	Granodiorite	Ulaan Uul Mount	46°26.64′	99°51.38′	540	80.2	722.0	0.321	0.708799	8	0.7063	6.15	39.66	0.0937	0.512196	4	−8.6	−1.5	−0.52	1210	1493
M99-04	Diorite	Daltyn-Am stock	46°29.04′	100°01.38′	250	34.0	935.8	0.105	0.705966	7	0.7056	5.04	26.73	0.1139	0.512434	3	−4.0	−1.3	−0.42	1093	1140
M99-05	Granite	Daltyn-Am stock	46°29.04′	100°01.38′	250	128.8	536.1	0.694	0.707945	7	0.7055	3.92	23.48	0.1010	0.512430	3	−4.1	−1.0	−0.49	974	1129
	Biotite					443.6	37.0	35.00	0.826099	7											
M99-06	Granite	Hangay batholith	46°49.35′	100°03.01′	237	213.2	228.3	2.700	0.716033	7	0.7069	3.46	21.38	0.0977	0.512448	5	−3.7	−0.7	−0.50	923	1096
M99-07	Granite	Hangay batholith	46°49.35′	100°03.01′	250	167.9	444.4	1.092	0.709261	8	0.7054	5.31	29.98	0.1072	0.512489	7	−2.9	−0.1	−0.46	946	1043
	Biotite					754.0	16.0	142.7	1.181446	7											
M99-08	Granite	Hangay batholith	46°49.35′	100°03.01′	237	200.7	238.3	2.435	0.715153	7	0.7069	3.56	22.89	0.0941	0.512400	3	−4.6	−1.5	−0.52	956	1168
M99-09	Granite	Hangay batholith	46°49.39′	99°58.26′	250	129.1	493.3	0.756	0.708054	7	0.7054	3.85	21.69	0.1074	0.512469	3	−3.3	−0.4	−0.45	976	1076
M99-10	Granitic dike	Hangay batholith	46°49.39′	99°58.26′	237	240.9	68.55	10.19	0.741230	8	0.7069	1.65	6.20	0.1610	0.512542	3	−1.9	−0.8	−0.18	1754	1032
M99-11	Metapelite	Dzag Series	46°42.75′	99°55.82′	600	109.6	130.4	2.431	0.723792	7	0.7030	5.13	29.23	0.1062	0.512111	3	−10.3	−3.3	−0.46	1470	1646
M99-12	Pelitic ss	Dzag Series	46°42.75′	99°55.82′	600	42.1	186.8	0.651	0.715145	7	0.7096	5.15	25.92	0.1200	0.512179	3	−9.0	−3.1	−0.39	1577	1557
M99-13	Microgranite	Hangay batholith	46°38.27′	100°17.68′	250	87.0	200.8	1.252	0.711396	6	0.7069	5.97	30.46	0.1185	0.512490	4	−2.9	−0.4	−0.40	1056	1057
M99-15	Granite	Nariyn Teel pluton	45°57.31′	101°25.74′	230	218.7	203.8	3.104	0.717449	7	0.7073	3.85	26.22	0.0887	0.512297	3	−6.7	−3.5	−0.55	1040	1325
M99-16	Granite	Nariyn Teel pluton	45°56.50′	101°31.41′	230	241.7	295.1	2.368	0.715777	7	0.7080	8.33	46.02	0.1094	0.512300	4	−6.6	−4.0	−0.44	1241	1349
M99-17	Granodiorite	Unnamed pluton	45°54.38′	102°22.70′	230	106.6	563.3	0.547	0.711982	7	0.7102	4.26	25.40	0.1014	0.512134	4	−9.8	−7.0	−0.48	1378	1603
M99-18	Granite	Unnamed pluton	47°16.70′	104°33.56′	120	177.2	261.0	1.962	0.711052	8	0.7077	5.68	30.20	0.1137	0.512450	4	−3.7	−2.4	−0.42	1067	1115
	Biotite					1112.8	22.5	146.5	0.955210	14											
M99-19	Ongonite	Ongonite type locality	47°02.84′	105°11.19′	120	2409	11.27	688.4	1.883164	12	0.7091	5.86	14.59	0.2427	0.512639	3	0.0	−0.7	0.23	−2714	988
	White mica 1					10035	10.07	5420	9.72657	8											
	White mica 2					10052	9.81	5718	10.19762	4											
M99-20	Ongonite	Ongonite type locality	47°02.84′	105°11.19′	120	3175	15.82	640.9	1.784810	11	0.6918	3.40	8.06	0.2549	0.512632	4	−0.1	−1.0	0.30	−1933	1016
M99-21	Ongonite	Ongonite type locality	47°02.84′	105°11.19′	120	2527	26.21	292.2	1.208771	10	0.7105	5.53	14.02	0.2383	0.512609	3	−0.6	−1.2	0.21	−3401	1030
M99-24	Aplite	Tour-qtz bearing aplite	46°59.63′	105°06.29′	120	467.3	6.55	217.2	1.264875	9	0.8944	0.67	3.30	0.1233	0.512540	4	−1.9	−0.8	−0.37	1028	984
M99-25	Granite	Ongonhairkhan Pluton	47°01.09′	105°05.20″	120	225.5	217.5	2.996	0.711366	8	0.7063	5.18	35.68	0.0878	0.512517	5	−2.4	−0.7	−0.55	767	972
M99-26	Granite	Ongonhairkhan Pluton	46°58.83′	105°08.90′	120	285.5	180.8	4.564	0.713941	6	0.7062	7.24	40.04	0.1092	0.512529	3	−2.1	−0.8	−0.44	906	982
	Biotite					1057	15.3	206.9	1.054745	7											

Note. $^{143}Nd/^{144}Nd$ ratios have been corrected for mass fractionation relative to $^{146}Nd/^{144}Nd = 0.7219$ and are reported relative to the La Jolla Nd standard = 0.511860 or Ames Nd standard = 0.511964. $^{87}Sr/^{86}Sr$ ratios have been corrected for mass fractionation relative to $^{86}Sr/^{88}Sr = 0.1194$ and are reported relative to the NBS-987 Sr standard = 0.710250. CHUR (chondritic uniform reservoir): $^{147}Sm/^{144}Nd = 0.1967$; $^{143}Nd/^{144}Nd = 0.512638$. Used in model age calculation, DM (depleted mantle): $^{147}Sm/^{144}Nd = 0.2137$; $^{143}Nd/^{144}Nd = 0.51315$. Blanks: Rb = 30 pg, Sr = 100 pg, Sm = 37 pg, Nd = 100 pg. TDM-1 = $1/\lambda * \mathrm{Ln}[1 + (0.51315 - (^{143}Nd/^{144}Nd)s)/(0.2137 - (^{147}Sm/^{144}Nd)s)]$. TDM-2 = $[(\varepsilon_{DM} - \varepsilon_{sample} + Q^* T_c^* (f_s - f_{cr}))/Q(f_{DM} - f_{cr})$, where $\varepsilon_{DM} = 10$, $f_{DM} = 0.086$, $f_{cr} = -0.4$, and $Q = 25.1'$.

The two-stage model age is obtained assuming that the protolith of the granitic magmas has a Sm/Nd ratio (or $f_{Sm/Nd}$ value) of the average continental crust (Keto and Jacobsen, 1987)

$$T_{DM}(2) = T_{DM1} - (T_{DM1} - t)(f_{cc} - f_s)/(f_{cc} - f_{DM}),$$

where $f_{cc}, f_s, f_{DM} = f_{Sm/Nd}$ values of the average continental crust, the sample and the depleted mantle, respectively. In our calculation, $f_{cc} = -0.4$ and $f_{DM} = 0.08592$ are used, and t =the intrusive age of granite.

Rb–Sr and Sm–Nd isochron ages were calculated using the regression programs of ISOPLOT (Ludwig, 1999). Input errors are $^{147}Sm/^{144}Nd = 0.2\%$, $^{143}Nd/^{144}Nd = 0.005\%$; $^{87}Rb/^{86}Sr = 2\%$, and $^{87}Sr/^{86}Sr = 0.005\%$. Analytical precisions for isotope ratio measurements are given as ± 2 standard errors ($2\sigma_m$), whereas the quoted errors in age and initial isotopic ratios represent ± 2 standard deviations (2σ).

Two samples were selected for zircon dating using a SHRIMP newly installed in the Chinese Academy of Geological Sciences, Beijing. U–Th–Pb analyses of the zircons were performed following standard procedures described by Williams (1998). The mass resolution used to measure Pb/Pb and Pb/U isotopic ratios was about 5000 during the analyses and the Pb/U ratios were normalised to those measured on the standard 572 Ma Sri Lanka zircon [SL13: $-(^{206}Pb/^{238}U = 0.0928)$]. The $^{206}Pb/^{238}U$ ages are considered to be the most reliable for concordant Phanerozoic zircons, because the low count rates on ^{207}Pb result in large statistical uncertainties, making the $^{207}Pb/^{206}Pb$ and $^{207}Pb/^{235}U$ ratios a less sensitive measure of age. Errors on individual analyses are based on counting statistics and are at the 1σ level. Errors on pooled analyses are quoted at 2σ or 95% confidence.

5. Petrographic and geochemical characteristics

The results of chemical analysis on 24 samples are given in Table 1. The principal major element characteristics may be summarized as follows: (1) In a K_2O vs. SiO_2 diagram (not shown), all samples plot in the high-K calc–alkaline series, except for a diorite of the Daltyn-Am stock. (2) In an A/NK vs. A/CNK plot, all rocks plot in the peraluminous field except the diorite and a granodiorite (M99-17). Three ongonite samples (M99-19, 20, 21) are highly peraluminous (Fig. 2a). (3) In the Q' vs. ANOR classification scheme of Streckeisen and Le Maitre (1979) most rocks belong to granites (monzogranite, syenogranite, and alkali feldspar granite), except one diorite (M99-04) and two granodiorites (M99-17 and M99-03; Fig. 2b). The ongonites are equivalent to alkali feldspar granites. The principal petrographic and geochemical characteristics of individual samples are described as follows.

Tsagaan Nuruu granite. This is an early Paleozoic two-mica granodiorite intrusive into the contact zone between the Bayonhongor Ophiolite and the Riphean sedimentary sequence of the Baydrag terrane. The analyzed samples (M99-01, -02) are medium-grained two-mica monzogranites, which have a similar mineralogical composition—subhedral zoned plagioclase, subhedral orthoclase (some with Carlsbad twins) and interstitial quartz and orthoclase. Myrmekites are common. Other essential minerals are brown biotite and muscovite. Accessory minerals include apatite, zircon and magnetite. Both samples are altered, leading to the formation of chlorite, magnetite, prehnite, sericite, pistacite and carbonate. No deformation is found. The two samples belong to a calc–alkaline series rich in K and strongly peraluminous. Note that the granite samples are very rich in Sr (1070–800 ppm) and Ba (1700–1580 ppm), their REE patterns are 'granitic' but with little Eu anomalies (Fig. 3a). The distinct negative anomalies in Nb(+Ta), P and Ti in primitive-mantle-normalized spidergrams (Fig. 4a) suggest their formation in an island arc (or continental arc) environment. Rikhter et al. (1994) have shown that the Tsagaan Nuruu pluton is surrounded by kyanite-sillimanite metamorphic rocks, forming a granite–metamorphic complex. They suggested that the granite could have been formed by palingenic processes involving partial melting of older magmatic rocks and metasediments. This appears to be supported by the present isotopic data.

Ulaan Uul granite. This is a pluton of red porphyritic granodiorite of the Ugalz intrusive complex. It is also intrusive into the Bayonhongor Ophiolite but is covered by upper Ordovician sediments. The analyzed sample (M99-03) came from the Ulaan Uul (= Red Mountain). It is a medium-grained porphyritic biotite granodiorite with rounded microgranular dark enclaves. The texture is granular, with euhedral megacrystals of K-feldspar. Plagioclase, quartz, orthoclase and biotite are the major constituent phases. Myrmekites are present. The average grain size is about 5 mm. Accessory minerals include apatite, zircon, titanite, ilmenite and allanite. Secondary minerals are sericite, chlorite, prehnite and pistacite. No deformation is observed. The sample belongs to a calc–alkaline series, slightly peraluminous. The trace element geochemical feature is very similar to that of the Tsagaan Nuruu granites. It has high Sr (680 ppm), high Ba (1340 ppm), and a similar REE pattern except twice as abundant (Fig. 3a). It exhibits the same negative anomalies in the spidergram (Fig. 4a).

Daltyn-Am stock. This is a small intrusion emplaced within the Bayanhongor ophiolite complex. Sample M99-04 is a medium-grained diorite containing augite, hornblende, and biotite, in addition to dominant plagioclase (andesine) which amounts to nearly 50%. Minor quartz ($\leq 3\%$) occurs as an interstitial mineral. Colored minerals represent the other half of the rock. Accessory minerals are ilmenite, magnetite, and apatite. Secondary minerals include chlorite, pistacite and rare carbonate. The rock is calc–alkaline, medium-K and strongly metaluminous (Fig. 3a). Sample M99-05 is a medium-grained monzogranite, composed of plagioclase, orthoclase (some perthite), interstitial quartz,

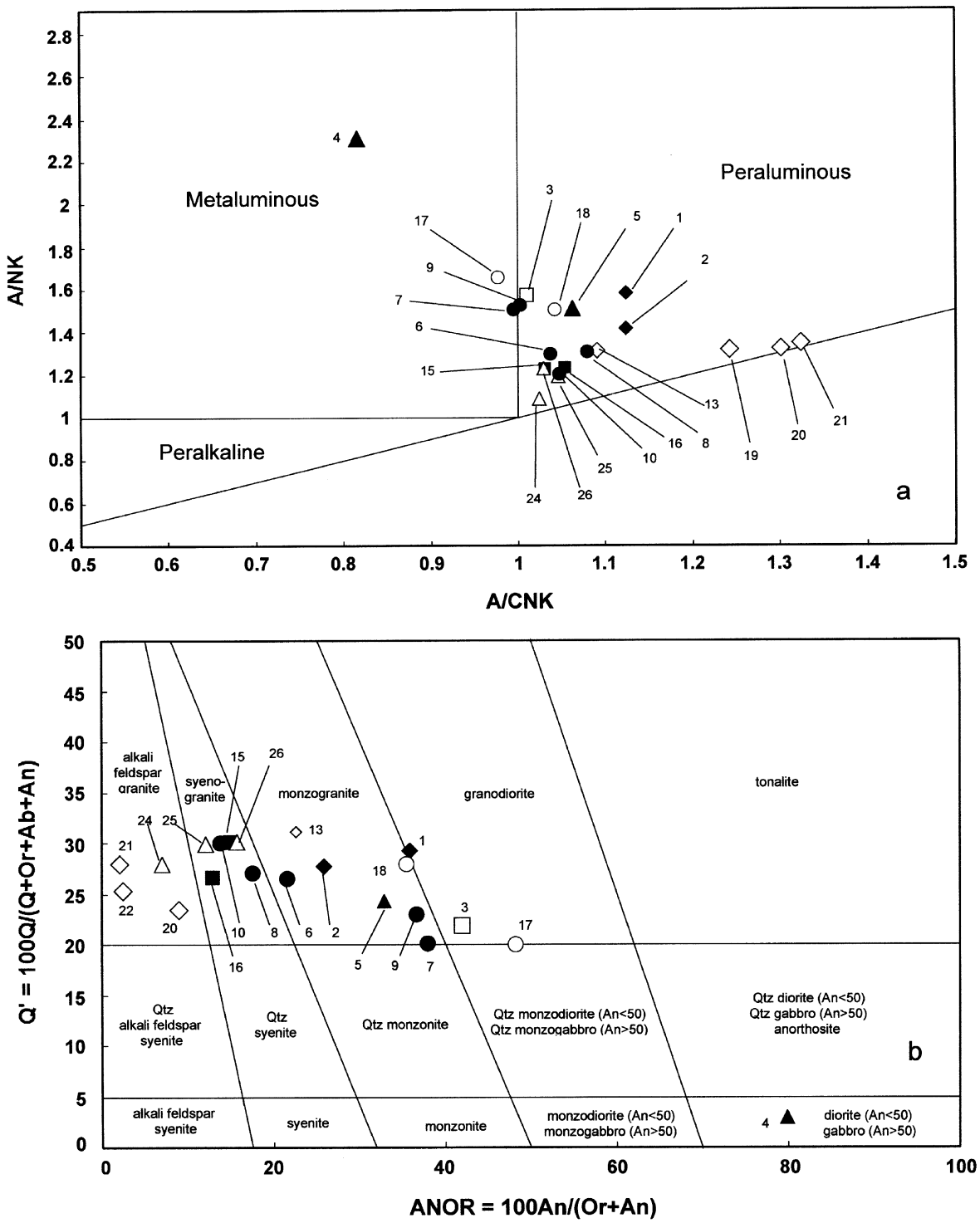

Fig. 2. (a) A/NK vs. A/CNK plot (Maniar and Piccoli, 1989) showing the peraluminous nature for most Mongolian granitoids. A = Al_2O_3, N = Na_2O, K = K_2O, C = CaO (molar proportion). (2) Normative compositions showing that most Mongolian granitoids belong to granites (s.s.), including monzogranite, syenogranite and alkali feldspar granite, based on the classification of Streckeisen and Le Maitre (1979). One diorite and two granodiorites are also found. The diorite is metaluminous.

green hornblende and minor brown biotite. Low-temperature hydrothermal alteration products include chlorite, pistacite and sericite. This is calc-alkaline, rich in K and slightly peraluminous. The two samples appear to belong to the same cogenetic series. The two samples have similar LREE abundances (ca. 100 × chondrites) but diverge in HREE. They show slight positive Eu anomalies in REE patterns (Fig. 3a) and the same kind of negative anomalies

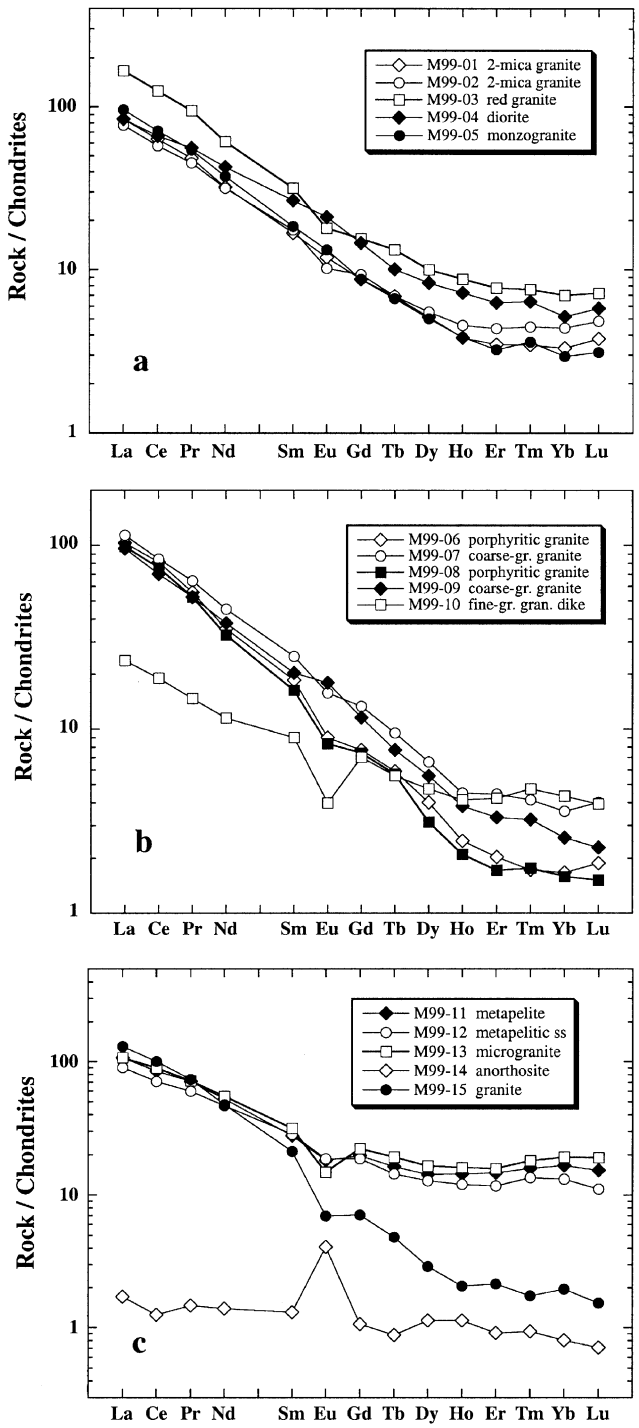

Fig. 3. REE patterns of Mongolian granitoids. The chondrite values are from Masuda et al. (1973) divided by 1.2. Sample M99-14 is an anorthosite from the Bayanhongor ophiolite complex. The rock is not further discussed in the text.

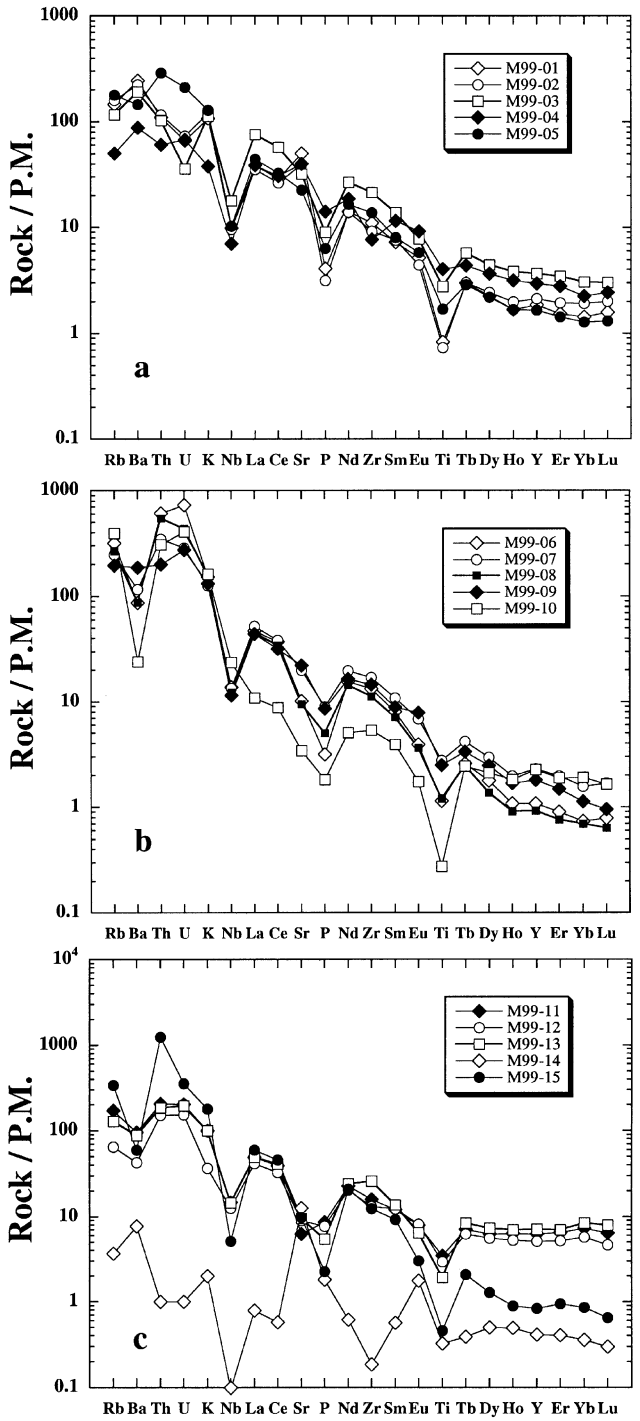

Fig. 4. Spidergrams of the granitoids corresponding to Fig. 3. The values of primitive mantle (P.M.) are from Sun and McDonough (1989).

in Nb–P–Ti in spidergrams (Fig. 4a) as the preceding samples.

Hangay batholith. Five Hangay samples were collected from a locality close to the Dzag formation (pelites and sandstones) and about 20 km from the Bayanhongor ophiolite zone. They include two coarse-grained granitoids (the main phase of the batholith), two porphyritic dikes and one fine-grained aplite. The two main-phase samples (M99-07, -09) are biotite–hornblende monzogranites. They contain zoned plagioclase, microcline and interstitial quartz. Accessory minerals include titanite, zircon, apatite, allanite and rare opaques. Though weathered in the outcrop, the samples are surprisingly fresh with little alteration in the thin sections. Chlorite and sericite are present only in tiny

amount in M99-07, and chlorite, zoisite and pistacite are found in M99-09. Both samples do not show post-magmatic deformation. They are of calc–alkaline series and about saturated in alumina (A/CNK about 1, Fig. 2a). We note that the chemical compositions and REE patterns of the main phase granites are quite similar to that of the Daltyn-Am stock (Table 1, Figs. 3a, b and 4a, b). Also, they have almost identical isotopic compositions and Sm–Nd model ages (Table 2). The principal characteristics of the REE patterns are their low HREE abundances and small or no Eu anomalies (Figs. 3a and b).

The two porphyritic dike samples (M99-06, -08) are biotite micro-granites. Phenocrysts of quartz and feldspars, often up to 5 mm long, and biotite are set in a fine-grained groundmass. Both samples have similar mineralogy. Oligoclase is subhedral and shows rythmic zoning; K-feldspar is anhedral and contains plagioclase and biotite as inclusions. Quartz is rounded and engulfed. Biotite is rich in tiny inclusions of accessory minerals—zircon, titanite and opaques. The sample is very fresh and contains little alteration product. The groundmass is mainly composed of quartz and feldspars. Both samples have about 72% SiO_2 contents, and belong to the high-K calc–alkaline series, and are peraluminous. The two samples have highly fractionated REE patterns with small negative Eu anomalies. The Hangay granites are also enriched in Rb and Th–U, but depleted in Nb, P and Ti as shown in the spidergrams (Fig. 4b). The geochemical characteristics suggest an enriched mantle as the source for the parental magma(s) of the Hangay batholith.

The fifth sample (M99-10) is a medium-grained leucogranitic dike containing a small amount of biotite and garnet (Bt $\gg$ Grt). The light-colored minerals include albite, microcline and quartz. Biotite is very dark. Alteration products are chlorite, sericite, secondary muscovite, zoisite, pistacite and hematite. The rock is very high in SiO_2 (75%) and is distinguished from other Hangay samples by its much lower total REE but the highest HREE abundances and large negative Eu anomaly (Fig. 3b). Its REE pattern is completely different from other Hangay granitoids. The sample is also highly enriched in Rb and U–Th in the spidergram (Fig. 4b).

A fine-grained felsic sample (M99-13), collected by Kröner and Windley, is a two-mica micro-granite composed of small phenocrysts of quartz and feldspars (orthoclase and albite) set in a groundmass. The groundmass contains very tiny red biotite and some secondary muscovite. Very rare epidote and opaques are also present. Its Sr and Nd isotopic compositions are very similar to those of the Hangay granitoids just described above; we assign the same age of 250 Ma for this sample.

Dzag series. Two samples were collected from the Cambro-Ordovician turbidite sequence. Sample M99-11 is a very fine-grained calc-schist, composed of alternating quartz-rich, muscovite-rich and dolomite layers. Small amount of albite is present in quartz-rich layers. Other accessory minerals include apatite, zircon, and green tourmaline. The rock is strongly schistose, and the paragenesis indicates a lower greenschist facies. Sample M99-12 is a fine-grained calcareous meta-sandstone, composed of quartz, carbonate, albite, muscovite, chlorite, and opaques. The deformation is moderate and the paragenesis also suggests a lower greenschist facies. The two samples have very similar REE patterns and trace element spidergrams (Fig. 3c and 4c). Most surprisingly, the total trace abundance pattern of the Dzag metapelite sample (Fig. 5) is almost identical to the average post-Archean shale (Taylor and McLennan, 1985, 1995) or Phanerozoic cratonic shale (Condie, 1993). It suggests that the Dzag metasediments represent a well mixed and homogenized sample, probably derived from a large area covering Proterozoic and Archean terranes that existed before the formation of the Paleozoic island arcs. The structural analysis of Buchan et al. (2001) suggested that the Dzag sequence may have been part of a passive margin of a continent located beneath the sedimentary cover of the Hangay region. This suggestion is compatible with the present geochemical analysis.

Nariyn Teel pluton (M99-15, -16). Sample M99-15 is a coarse-grained pink biotite leuco-syenogranite with dark microgranular enclaves. Oligoclase, microcline and quartz are present in about equal proportions. Brown biotite is the only colored mineral in major phases. Allanite, apatite and zircon represent the accessory phases. The rock has been hydrothermally altered, producing sericite, muscovite, chlorite, clinozoisite, pistacite and titanite. It has a highly fractionated REE pattern. Its $(La/Yb)_N$ ratio of almost 70 is the highest among all the samples studied. Sample M99-16 is a porphyritic coarse-grained biotite syenogranite. It has the same mineralogy as M99-15 except that oligoclase and microcline are present as megacrysts up to several centimeter long and myrmekitic quartz is more frequent. Biotite is entirely transformed to chlorite. Accessory minerals include allanite, apatite, zircon, titanite, and magnetite. Its REE pattern is high and fractionated with a large negative Eu anomaly (Fig. 6a). K, Rb, U and Th are strongly enriched in the spidergram (78a). Both samples are high-K calc–alkaline and slightly peraluminous. The Nariyn Teel pluton was believed to have a Permian age and forms a part of the Hangay batholith. The present zircon U–Pb SHRIMP result gave a Triassic age (230 Ma; see later).

Granites of unnamed massifs (M99-17, 18). Sample M99-17 is a medium-grained granodiorite with microgranular dark enclaves. Plagioclase shows a clear zoning, and quartz and orthoclase are interstitial phases. Mafic minerals include biotite and hornblende. Accessory phases are zircon, apatite, ilmenite, titanite. Sericite, chlorite and epidote are alteration products. This sample is high-K calc–alkaline and metaluminous. Its REE pattern is very similar to that of the Hangay granitoids, highly fractionated with absence of a Eu anomaly (Fig. 6a). Sample M99-18 is

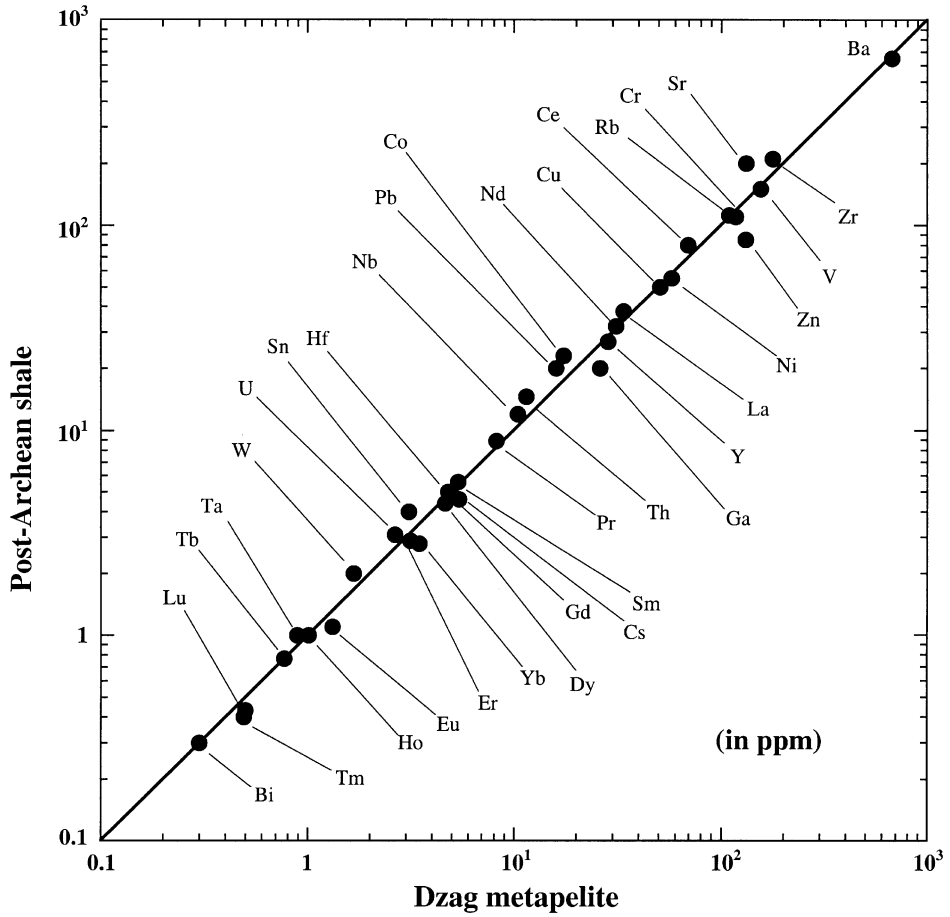

Fig. 5. The close similarity in chemical composition between the Cambro-Ordovician Dzag metapelite and the average post-Archean shale of Taylor and McLennan (1985). The concentrations of Cs, Rb, Nb, Ta and W are from McLennan (2001) for the upper continental crust.

a medium-grained monzogranite. It is very fresh and shows no sign of alteration except a trace amount of hematite. The texture is granular, with plagioclase somewhat zoned and K-feldspar slightly microclined. Quartz is interstitial. Biotite is brown and very fresh. The main accessory minerals are apatite and zircon. The sample shows no sign of deformation. It is also high-K calc–alkaline but slightly peraluminous. In contrast to M99-17, its REE pattern is less fractionated but shows a large negative Eu anomaly (Fig. 6a).

Ongonites (M99-19, 20, 21). Ongonite is a magmatic rock with a peculiar chemical composition (Kozakov et al., 2001; Stemprok, 1991; Antipin et al., 1999). It was originally defined by Kovalenko et al. (1970) as a topaz-bearing albite–quartz keratophyre, highly enriched in Li (0.2–0.3%) and F (up to 4%). The phenocrysts include K-feldspar, amazonite, albite, quartz, topaz, and Li-mica. The matrix contains the same mineralogy. Accessory minerals include spessartine, monazite, zircon, pyrochlore, etc. Chemically, it was also considered to be a highly differentiated S-type or ilmenite series granitoid (Stemprok, 1991), but we disapprove of this S-type designation based on the chemical and isotopic argument presented below.

Three samples were collected from the type locality where Kovalenko first identified this rock type. The outcrop is a white dike (ca. 2–3 m) cutting silty sandstone. The closest granitic pluton is about 10 km away. The ongonite dikes in this region are spatially associated with a tungsten (wolframite) stockwork deposit of the Ongonhaikhan ore field (Kovalenko et al., 1970; Stemprok, 1991). Sample M99-19 represents the porphyritic inner part of the dike, M99-20 is an aphyric chilled margin, whereas M99-21 is intermediate between the two. In sample M99-19 rounded grey quartz phenocrysts, about 0.5–3 mm long, and rare euhedral light green amazonite of 1–3 mm are present. Other phenocrysts include albite, orthoclase, white mica (Li-phengite or zinnwaldite). Albite crystals are in laths or aggregates, and are surrounded by orthoclase and quartz. Occasionally, they show a snow-ball texture commonly observed in rare-metal granites (Jahn et al., 2001). The groundmass is granular with a large variation of grain size (average ca. 0.05 mm). It is mainly composed of quartz, feldspar, white mica, and a small amount of topaz, fluorite and ilmenite. Samples M99-20 (aphanitic) and M99-21 (porphyritic) have the same mineralogy as M99-19. No deformation has been observed. All ongonites are chemically equivalent to alkali feldspar granites and highly peraluminous (Fig. 2a; Fig. 7).

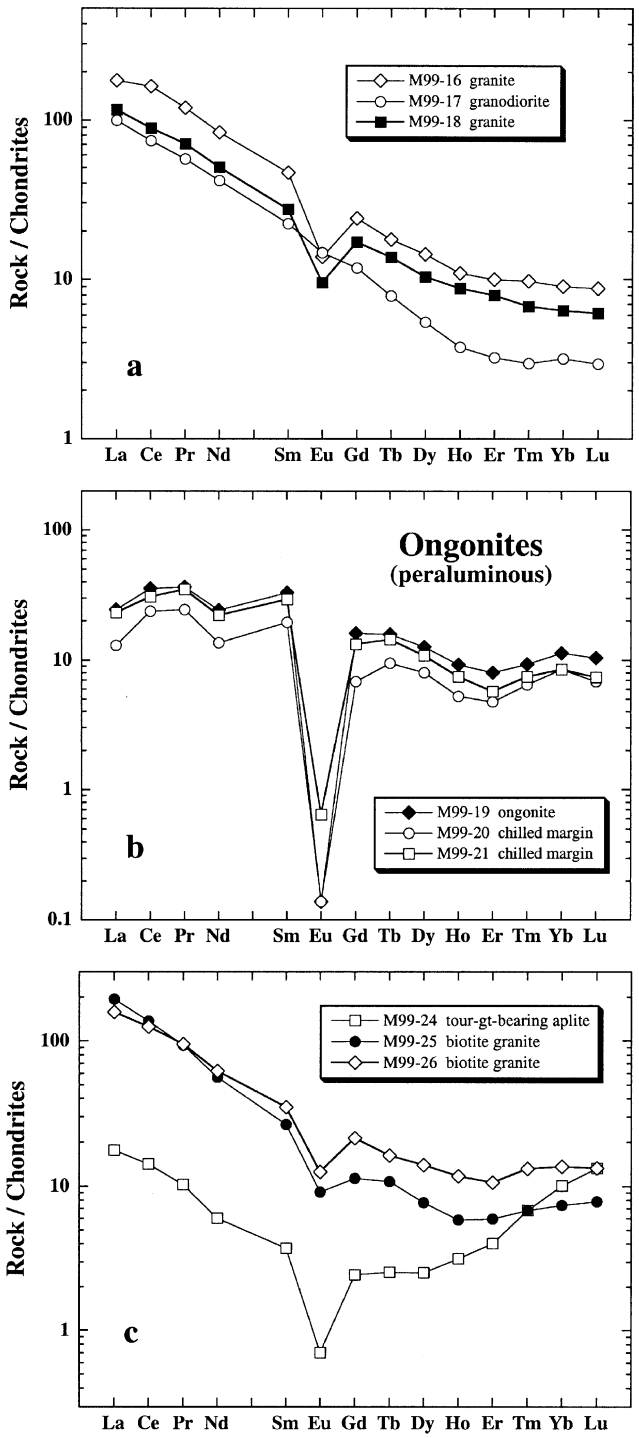

Fig. 6. REE patterns of Mongolian granitoids. Three ongonites show tetrad effect with large negative Eu anomalies on their REE distribution patterns. Sample M99-24 (aplite) shows an incipient development of the tetrad effect.

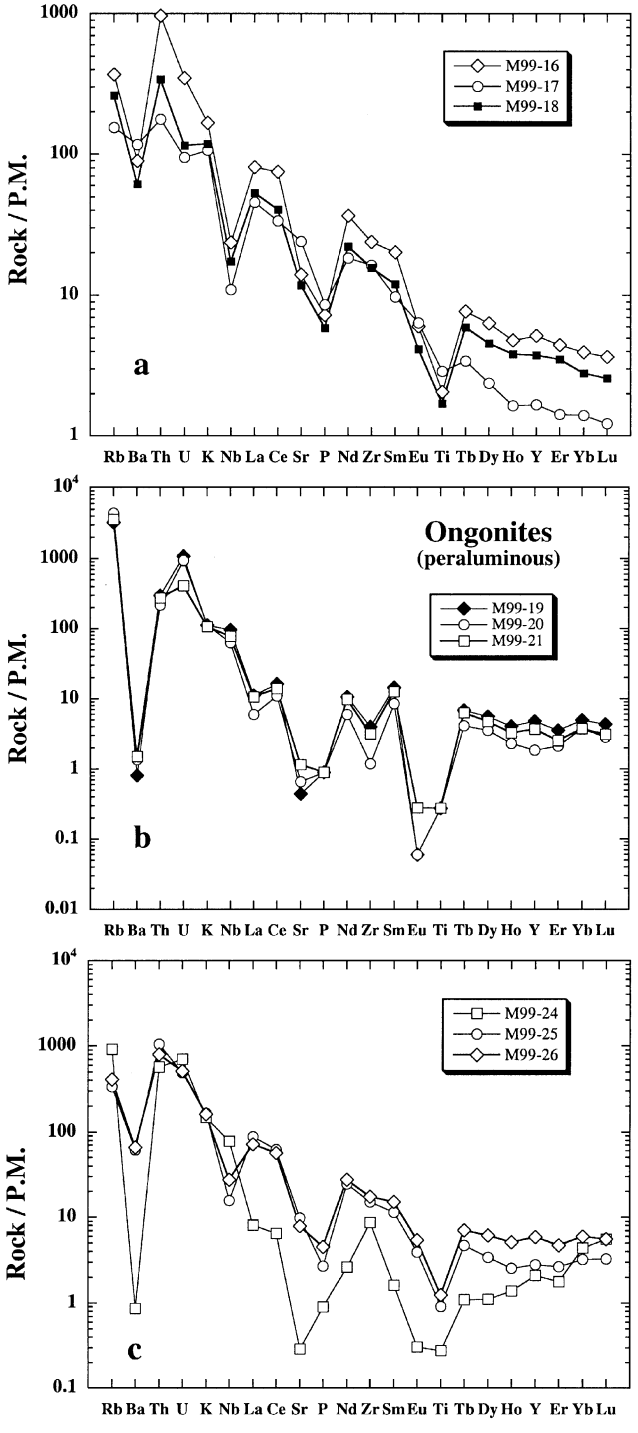

Fig. 7. Spidergrams of the granitoids corresponding to Fig. 6. Note the close similarity of the patterns between ongonites and aplite (b and c).

The most spectacular chemical feature (Table 1) is the very high Rb (2100–2800 ppm) and very low Sr (9–25 ppm), leading to extremely high Rb/Sr ratios (220–93). In addition, the rocks contain unusually high concentrations of Ga (60–70 ppm), Sn (30–45 ppm), Bi (40–80 ppm), Ta (113–76 ppm), Nb (69–45 ppm). The less-than-unity Nb/Ta ratios (0.5–0.7) are exceptional in magmatic rocks (Table 1). Moreover, the rocks show tetrad REE patterns with huge negative Eu anomalies (Fig. 6b) and non-charge-and-radius-controlled (non-CHARAC, Bau, 1996) trace element behavior (Fig. 8), which are only observed in highly differentiated acid magmas in which the late stage magmatic liquid had a strong interaction with hydrothermal

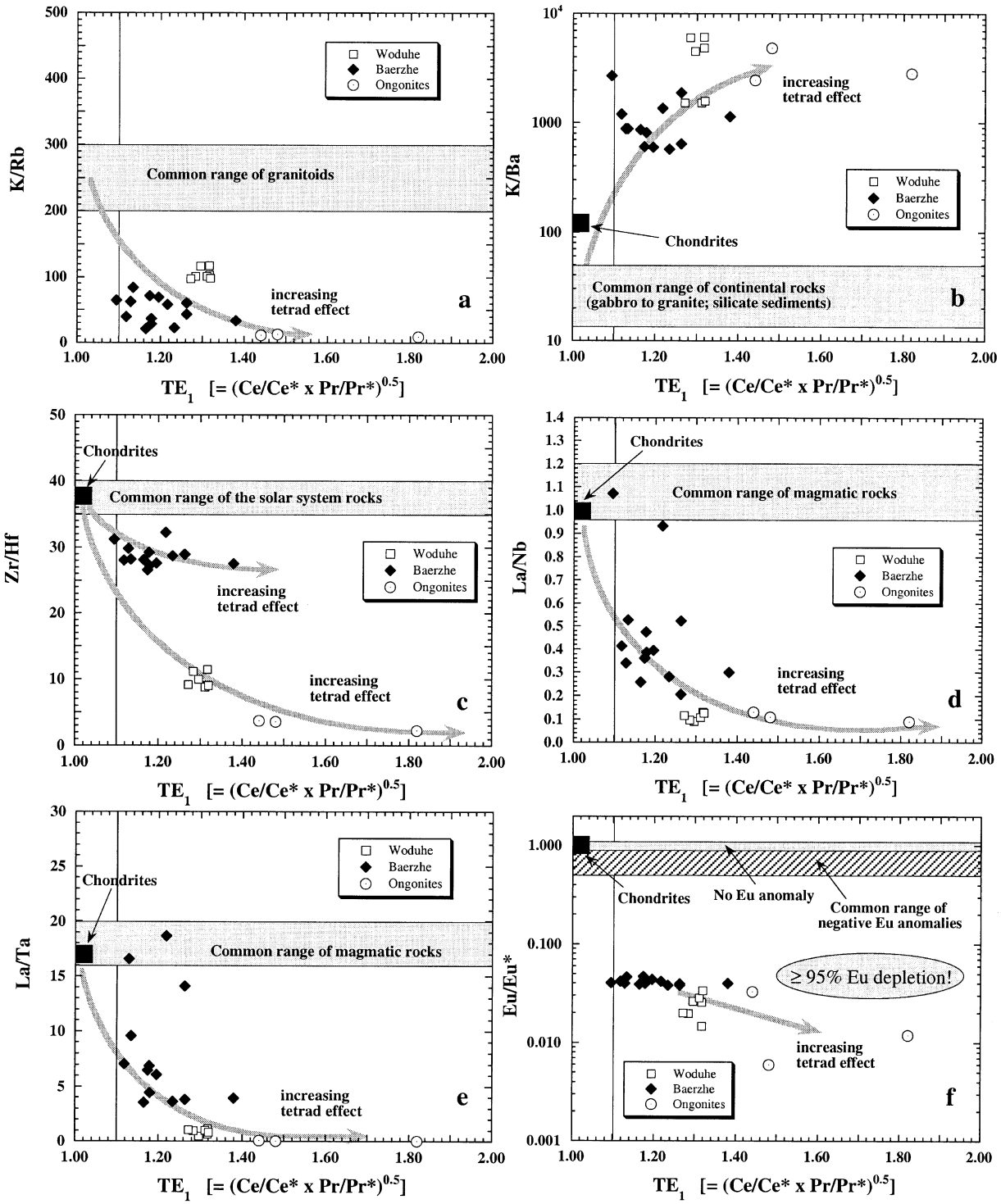

Fig. 8. Non-CHARAC trace element behavior in granitoids with tetrad REE patterns. The data of Woduhe and Baerzhe are from Jahn et al. (2001). The ongonites show the highest tetrad effect and deviation from the CHARAC behavior of these elements.

fluids (Masuda and Akagi, 1990; Bau, 1996; Irber, 1999; Jahn et al., 2001). Granitoids with tetrad REE patterns have recently been documented in three localities in NE China (Jahn et al., 2001; Wu et al., 2002) and one locality in the Junggar terrane of northern Xinjiang (Chen and Jahn, 2003). With such unusual non-CHARAC behavior of trace elements and the high differentiated nature, assignment of tectonic setting or classification of petrogenetic types (I-, S-, etc.) based on trace element abundances for this kind of rock is no longer valid (Jahn et al., 2001).

Ongonhairkhan pluton (M99-25, 26). The rocks are coarse-grained biotite syenogranites. They represent the main facies of the Ongonhairkhan pluton. The outcrop shows well-developed exfoliation. The pluton is considered to be emplaced in the same period as the ongonites and formed in an intra-continental environment (Mongolian Guidebook, 1999). The two samples are composed essentially of plagioclase, orthoclase and quartz. Myrmekites are abundant. Brown biotite is the only colored mineral and it is somewhat chloritized. A few laths of secondary muscovite are present. Accessory minerals include allanite, titanite, ilmenite, apatite and zircon. The two samples have high REE abundances of a typical granitic pattern with distinct negative Eu anomalies. They also have high Th (59–45 ppm) and U (6–7 ppm) concentrations (Table 1).

Aplite (M99-24). This aplitic dike cuts shaly sediments, and is believed by some workers to be the border facies of the Ongonhairkhan pluton. The texture is fine-grained but granular, and its principal minerals are albite, quartz and microcline. Minor phases include biotite (residual), garnet, tourmaline (zoned) and interstitial non-colored fluorite. It is high-K calc–alkaline and slightly peraluminous. Like the ongonites, it is classified as an alkali feldspar granite. It has a concave-shaped REE pattern with large negative Eu anomaly (Fig. 6c). The REE pattern and other trace element ratios (K/Rb = 63, Rb/Sr = 96, K/Ba = 6076, Zr/Hf = 10, La/Nb = 0.1, La/Ta = 1; Table 1) appear to indicate an incipient stage of development of a tetrad REE pattern. The spidergram of this aplite is very comparable with that of ongonites (Fig. 8b and c).

6. Assessment of intrusive ages

The results of Rb–Sr and Sm–Nd isotopic analyses are presented in Table 2, and the SHRIMP age data are given in Table 3. We have not conducted a systematic age study on individual samples, but we need to use probable age values to obtain initial isotopic ratios for the ensuing discussion. Except for a few new ages obtained here, our estimate of intrusive ages is mainly based on literature data (Mongolian Guidebook, 1999 and references therein) and the isotope information obtained in this work. Our assessment of intrusive ages is as follows.

Tsagaan Nuruu granite. A gabbro of the Bayanhongor Ophiolite was dated at 569 ± 21 Ma by Kepezhinskas et al. (1991) using the Sm–Nd mineral isochron technique. Consequently, the Tsagaan Nuruu granite that is intrusive into the ophiolite must be younger than 570 Ma. Earlier dating attempts produced K–Ar ages ranging from 550 to 470 Ma. The result of zircon SHRIMP dating is shown in Fig. 9. Because the size of zircons in this sample is very small (≤20 μm), the ion beam spot size was reduced to 15 μm, which produced a weaker ion intensity and poorer precision for the measurement. Nevertheless, the data indicate a very complex history. A statistical analysis of 14 near-concordant grains yielded a $^{206}Pb/^{238}U$ age of 514 ± 10 Ma (Fig. 9b), which is considered as the time of the pluton emplacement. The other data points indicate the presence of inherited zircons of probable middle-to-early Proterozoic ages. The calculated initial $^{87}Sr/^{86}Sr$ ratios ($= I_{Sr}$) are about 0.708, and $\varepsilon_{Nd}(T)$ values about −7.0 (Table 2). All these point to the idea that an older Baydrag crustal component must have played a significant role in the petrogenesis of the Tsagaan Nuruu granite.

Ulaan Uul red granite. Because of its intrusive nature with respect to the Bayanhongor Ophiolite and its underlying relationship with upper Ordovician sediments, its emplacement age is constrained to be 560–450 Ma. A biotite K–Ar age of 469 ± 9 Ma was obtained by Takahashi et al. (2000), whereas two zircon ages of 539 ± 1 Ma (for M98/B7) and 545 ± 2 Ma (for M97/77) were obtained by the lead evaporation method by Buchan et al. (2002) on two red granites collected from the same locality as the present Ulaan Uul granite. Petrographic description, chemical data, and Sr–Nd isotopic analyses on the two samples confirm that we have analyzed samples from the same red granite body. We adopt 540 Ma as the intrusive age for the following discussion. The red granite has similar geochemical characteristics as the Tsagaan Nuruu granite, only with high overall REE and trace element abundances (Figs. 3a and 4a). Its calculated I_{Sr} is 0.7063 and $\varepsilon_{Nd}(T)$ value is −1.5. Together with its younger Sm–Nd model age (T_{DM}) of 1.2–1.5 Ga (Table 2), this suggests that the influence of an old crustal component is significant but reduced relative to the Tsagaan Nuruu granite.

Daltyn-Am stock. Though it is intrusive into the Bayanhongor ophiolite complex, its emplacement age is not well constrained. Our two Rb–Sr analyses allow a rough estimate of a two point whole-rock isochron age of 236 ± 8 Ma. A biotite analysis (M99-05) gave a biotite-WR isochron age of 242 ± 5 Ma, with $I_{Sr} = 0.7056$. If the biotite is combined with the two WR data, an isochron of 241 ± 4 Ma, with $I_{Sr} = 0.70567 \pm 0.0003$ (MSWD = 1.5) was obtained. Takahashi et al. (2000) published five Rb–Sr whole-rock isotope analyses and they obtained an isochron age of 275 ± 12 Ma using four data points (P97-62 excluded). A re-calculation of their data assuming input errors of 2% for $^{87}Rb/^{86}Sr$ and 0.005% for $^{87}Sr/^{86}Sr$ yielded 269 ± 44 Ma (MSWD = 7.8). If our two analyses are combined with the five of Takahashi et al. (2000), a seven point 'errorchron' age of 248 ± 37 Ma is obtained (MSWD = 13). Because the biotite age of 242 Ma is considered as the time of magmatic cooling down to its blocking temperature of 300–400 °C, we assume an age of 250 Ma for the intrusive event. In so doing, the calculated I_{Sr} (ca. 0.705) and $\varepsilon_{Nd}(T)$ values (0 to −1) as well as Sm–Nd model ages (about 1000 Ma) are very similar to those of the main phase granites of the Hangay batholith (Table 2) which has a proven emplacement age of 250 Ma (see below). Consequently, we consider the Daltyn-Am stock a part of the Hangay batholith.

Table 3
SHRIMP U–Pb–Th data for zircons from the Tsagaan Nuruu and Nariyn Teel Plutons

Spot	U (ppm)	Th (ppm)	$^{232}Th/^{238}U$	$^{206}Pb_c$(%)	Total $^{238}U/^{206}Pb$	± %	Total $^{207}Pb/^{206}Pb$	± %	$^{238}U/^{206}Pb$	± %	$^{207}Pb^*/^{206}Pb^*$	± %	$^{207}Pb^*/^{235}U$	± %	$^{206}Pb^*/^{238}U$	± %	Error corr	$^{206}Pb/^{238}U$ Age(Ma)
M99-01-1	560	649	1.20	0.24	11.99	5.2	0.05947	1.2	11.71	3.3	0.05732	1.2	0.675	3.5	0.0854	3.3	0.936	515 ± 32
M99-01-2	108	61	0.58	1.07	11.11	5.3	0.0657	2.5	10.94	3.4	0.0572	2.9	0.720	4.5	0.0914	3.4	0.758	550 ± 31
M99-01-3	206	92	0.46	0.50	3.08	5.2	0.1548	0.67	3.08	3.3	0.1349	0.82	6.04	3.4	0.325	3.3	0.970	1771 ± 88
M99-01-4	518	425	0.85	–	11.23	2.8	0.0741	2.0	10.89	2.8	0.0977	1.5	1.237	3.2	0.0918	2.8	0.885	566 ± 17
M99-01-5	574	216	0.39	3.14	5.44	2.8	0.09012	0.70	5.62	2.8	0.06504	1.1	1.596	3.0	0.1780	2.8	0.929	1056 ± 30
M99-01-6	837	604	0.75	–	12.98	2.9	0.0781	2.4	12.79	2.9	0.0896	2.1	0.966	3.6	0.0782	2.9	0.814	485 ± 15
M99-01-7	1063	211	0.20	−0.01	8.29	2.9	0.0723	2.0	8.29	2.9	0.0723	2.0	1.203	3.5	0.1206	2.9	0.815	734 ± 20
M99-01-8	312	16	0.05	0.11	3.38	3.3	0.1212	1.6	3.38	3.3	0.1204	1.6	4.91	3.6	0.2959	3.3	0.901	1671 ± 49
M99-01-9	3825	3085	0.83	51.84	19.12	2.8	0.4684	1.3	39.7	2.8	0.043	38	0.148	39	0.02518	2.8	0.072	160 ± 23
M99-01-10	32	13	0.43	9.66	11.18	6.0	0.106	9.5	12.38	6.0	0.025	45	0.28	45	0.0808	6.0	0.134	501 ± 40
M99-01-11	770	89	0.12	1.05	9.96	2.9	0.0649	2.1	10.07	2.9	0.0564	2.4	0.773	3.8	0.0994	2.9	0.764	611 ± 17
M99-01-12	148	59	0.41	1.74	11.63	3.5	0.0659	5.1	11.84	3.5	0.0518	6.7	0.603	7.5	0.0845	3.5	0.460	523 ± 19
M99-01-13	91	56	0.63	2.88	12.63	4.0	0.0721	9.4	13.00	4.0	0.0486	14	0.516	15	0.0769	4.0	0.266	478 ± 21
M99-01-14	124	111	0.92	4.23	13.14	3.7	0.0713	6.2	13.72	3.7	0.0364	13	0.365	13	0.0729	3.7	0.281	453 ± 21
M99-01-15	666	563	0.87	−0.23	11.83	2.9	0.0671	2.0	11.80	2.9	0.0690	1.9	0.806	3.5	0.0847	2.9	0.834	524 ± 17
M99-01-16	170	72	0.44	4.20	7.10	3.2	0.1105	2.4	7.41	3.2	0.0774	3.6	1.441	4.8	0.1350	3.2	0.663	816 ± 28
M99-01-17	321	617	1.99	1.68	11.54	3.0	0.0685	2.8	11.74	3.0	0.0549	3.6	0.644	4.7	0.0852	3.0	0.642	527 ± 23
M99-01-18	1505	422	0.29	0.61	25.57	2.8	0.0524	2.2	25.73	2.8	0.0475	2.4	0.2544	3.7	0.0389	2.8	0.762	246 ± 7.2
M99-01-19	589	345	0.61	0.32	11.34	2.9	0.0661	2.0	11.38	2.9	0.0636	2.1	0.770	3.6	0.0879	2.9	0.805	543 ± 17
M99-01-20	806	893	1.14	0.82	12.24	2.9	0.0619	1.9	12.34	2.9	0.0552	2.2	0.617	3.6	0.0810	2.9	0.798	502 ± 17
M99-01-21	657	467	0.73	0.26	11.26	2.9	0.0629	1.9	11.29	2.9	0.0608	2.0	0.743	3.5	0.0886	2.9	0.821	547 ± 17
M99-01-22	338	41	0.13	1.17	9.37	3.0	0.0709	2.4	9.48	3.0	0.0616	2.8	0.895	4.1	0.1055	3.0	0.736	646 ± 19
M99-01-23	769	160	0.21	2.10	6.03	2.8	0.1062	10	6.16	2.8	0.0899	1.2	2.011	3.1	0.1622	2.8	0.917	969 ± 27
M99-01-24	457	106	0.24	1.17	12.05	2.9	0.0659	2.4	12.19	2.9	0.0565	2.9	0.639	4.1	0.0820	2.9	0.715	508 ± 15
M99-01-25	242	72	0.31	1.99	11.77	3.1	0.0707	5.4	12.01	3.1	0.0547	7.1	0.627	7.7	0.0832	3.1	0.404	515 ± 17
M99-01-26	522	90	0.18	−0.01	10.80	2.9	0.0661	2.2	10.80	2.9	0.0662	2.2	0.845	3.7	0.0926	2.9	0.797	571 ± 16
M99-01-27	223	249	1.15	1.21	12.49	3.5	0.0682	3.6	12.64	3.5	0.0584	4.3	0.637	5.6	0.0791	3.5	0.629	491 ± 21
M99-01-28	889	645	0.75	0.08	12.41	2.9	0.0619	3.3	12.42	2.9	0.0612	3.4	0.680	4.4	0.0805	2.9	0.649	499 ± 16
M99-01-29	446	62	0.14	−0.26	8.96	3.0	0.0671	2.3	8.93	3.0	0.0692	2.2	1.068	3.7	0.1119	3.0	0.800	684 ± 20
M99-16-1	353	12	0.03	0.57	28.2	5.2	0.0528	2.4	27.50	3.3	0.0514	2.5	0.258	4.2	0.0364	3.3	0.802	224 ± 12
M99-16-2	699	273	0.40	0.65	27.4	5.2	0.05302	1.7	26.44	3.3	0.05919	1.6	0.309	3.6	0.0378	3.3	0.904	233 ± 13
M99-16-3	1302	342	0.27	0.39	26.8	5.2	0.05308	1.2	26.15	3.3	0.05113	1.2	0.2696	3.5	0.0382	3.3	0.936	236 ± 13
M99-16-4	1273	664	0.54	0.14	28.1	5.2	0.05081	1.4	27.10	3.3	0.05947	1.2	0.303	3.5	0.0369	3.3	0.942	228 ± 13
M99-16-5	1985	192	0.10	0.17	27.0	5.2	0.05026	0.99	26.24	3.3	0.05046	0.99	0.2652	3.4	0.0381	3.3	0.957	235 ± 12
M99-16-6	844	1024	1.25	10.22	24.7	5.2	0.2060	3.6	29.30	3.3	0.0610	15	0.287	16	0.0341	3.3	0.209	211 ± 18
M99-16-7	628	936	1.54	0.54	27.3	5.3	0.05416	1.6	26.87	3.5	0.04566	2.0	0.2343	4.0	0.0372	3.5	0.870	229 ± 16
M99-16-8	1247	910	0.75	1.71	27.5	5.3	0.0761	3.3	27.80	3.4	0.0454	5.8	0.225	6.7	0.0360	3.4	0.501	222 ± 14
M99-16-8	379	433	1.18	0.15	29.9	5.2	0.0520	2.3	28.99	3.3	0.0553	2.2	0.263	4.0	0.0345	3.3	0.837	213 ± 14
M99-16-10	1090	418	0.40	0.55	26.4	5.2	0.05860	1.2	25.78	3.3	0.05669	1.2	0.303	3.5	0.0388	3.3	0.937	239 ± 13
M99-16-11	422	387	0.95	0.01	26.7	5.2	0.0512	2.4	26.97	3.3	0.0212	6.2	0.1085	7.0	0.0371	3.3	0.472	229 ± 15
M99-16-12	1994	402	0.21	0.26	27.4	5.2	0.05317	0.96	26.75	3.3	0.05108	10	0.2633	3.4	0.0374	3.3	0.956	231 ± 12
M99-16-13	462	202	0.45	1.12	26.1	5.2	0.0554	2.4	25.70	3.3	0.0475	2.8	0.255	4.4	0.0389	3.3	0.758	240 ± 13
M99-16-14	1518	536	0.36	0.37	26.4	5.2	0.05213	1.1	25.59	3.3	0.05544	1.0	0.299	3.4	0.0391	3.3	0.955	241 ± 13

(*continued on next page*)

Table 3 (*continued*)

Spot	U (ppm)	Th (ppm)	$^{232}Th/^{238}U$	$^{206}Pb_c$(%)	Total $^{238}U/^{206}Pb$	± %	Total $^{207}Pb/^{206}Pb$	± %	$^{238}U/^{206}Pb$	± %	$^{207}Pb^*/^{206}Pb^*$	± %	$^{207}Pb^*/^{235}U$	± %	$^{206}Pb^*/^{238}U$	± %	Error corr	$^{206}Pb/^{238}U$ Age(Ma)
M99-16-15	367	339	0.96	0.11	28.0	5.2	0.0528	2.2	27.72	3.3	0.0406	2.9	0.2019	4.4	0.0361	3.3	0.757	223 ± 14
M99-16-16	1634	401	0.25	0.13	27.5	5.2	0.05154	1.1	26.87	3.3	0.04989	1.1	0.2561	3.4	0.0372	3.3	0.946	230 ± 12
M99-16-17	117	109	0.96	−0.07	27.5	5.4	0.0511	4.3	27.07	3.5	0.0419	5.3	0.213	6.4	0.0369	3.5	0.551	228 ± 14
M99-16-18	1127	424	0.39	0.23	29.0	5.2	0.05188	1.5	28.27	3.3	0.04996	1.6	0.2437	3.6	0.0354	3.3	0.899	218 ± 12

Note. Errors are 1-sigma; Pb_c and Pb* indicate the common and radiogenic Pb portions, respectively. Error in standard calibration was 1.26% (not included in above errors but required when comparing data from different mounts). Common Pb corrected by assuming $^{206}Pb/^{238}U-^{208}Pb/^{232}Th$ age-concordance.

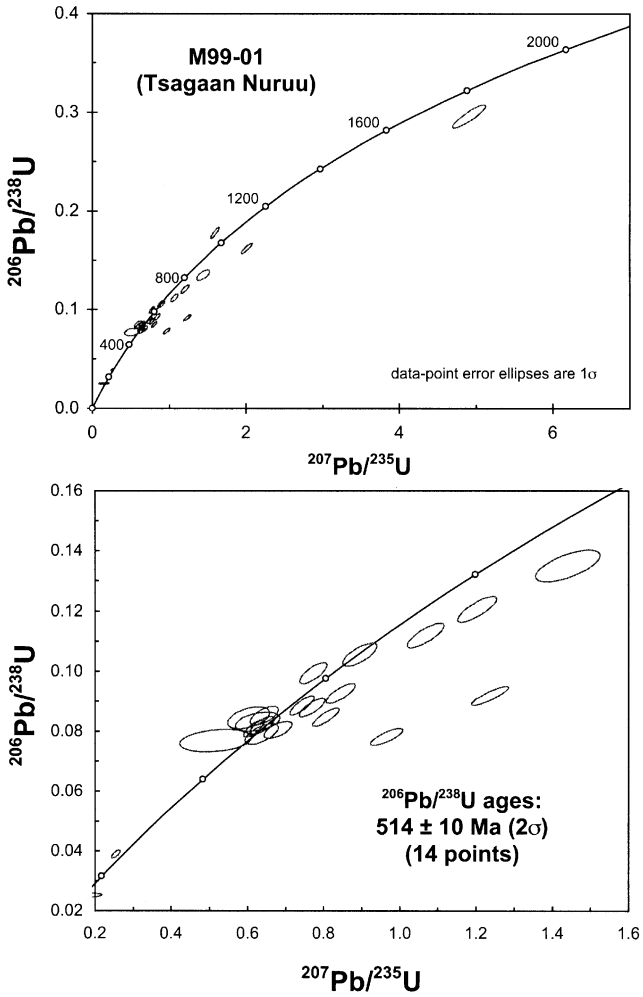

Fig. 9. SHRIMP U–Pb isotope analyses of zircons from a Tsagaan Nuruu granite (M99-01). (a) Inherited zircon components of Proterozoic ages are indicated from the data array; (b) an average $^{206}Pb/^{238}U$ age of 514 ± 10 Ma is obtained from 14 concordant data points.

Hangay batholith. The huge Hangay batholith was probably formed by multiple intrusions emplaced in several episodes. Budnikov et al. (1999) reported two zircon U–Pb ages (252 ± 3 and 253 ± 2 Ma) and four mica-WR isochron ages (220 ± 2 Ma, $I = 0.7056$; 228 = 2 Ma, 0.7051; 230 ± 22 Ma, 0.7058; 253 ± 2 Ma, 0.7058). They considered the U–Pb ages of about 250 Ma to best represent the emplacement time of the batholith. Their Rb–Sr mica ages could have resulted from a later thermal disturbance. We have only a limited analysis at present. The two coarse-grained granites provide a Rb–Sr date of 253 ± 22 Ma (two point isochron). An analysis of biotite from M99-07 (monzogranite) yielded a biotite-WR isochron age of 234 ± 5 Ma ($I_{Sr} = 0.7056$). Takahashi published five analyses on the Hangay granites which gave an age of 242 ± 22 Ma (MSWD = 11.8). If all data are combined, an age of 252 ± 35 Ma is produced (MSWD = 34). Takahashi et al. (2000) also gave a biotite K–Ar age of 249 ± 12 Ma. In the following discussion, we take 250 Ma for the intrusive age of the main phase of the Hangay batholith.

The three dike rocks crosscut the main phase granites. The Rb–Sr data of the dike rocks seem to define a good three-point isochron age of 237 ± 6 Ma with I_{Sr} = 0.7070 ± 0.0003 (MSWD = 0.01). However, we are not certain that they are truly cogenetic. Allowing the uncertainty in age, they have very similar calculated initial εNd(T) values (Table 2), hence suggesting that they could be comagmatic. In any case, we temporarily consider 237 Ma as the time of the dike emplacement.

Dzag series. K–Ar dating of white micas suggests that the greenschist facies metamorphism took place at 450 Ma (Kurimoto and Tungalag, 1998). The Dzag series is considered to represent a passive margin to the Hangay continent (Buchan et al., 1999, 2001). We assume 600 Ma for the deposition time of the Dzag series for the reason that the 570 Ma Bayanhongor Ophiolite was obducted onto the Dzag passive margin terrain (Buchan et al., 2001). The initial Sr isotope compositions for the two samples are 0.7030 and 0.7096, and ε_{Nd} (600 Ma) = −3.3 and −3.1, suggesting that the Dzag sediments have only a limited proportion of early Precambrian Baydrag gneisses. Their Nd model ages of about 1.5 Ga indicate the dominance of Proterozoic rocks (likely Neoproterozoic to Eo-Cambrian) in their source terrains.

Nariyn Teel pluton (M99-15,16) and unnamed stocks (M99-17,18). The Nariyn Teel pluton was believed to be emplaced in the Permian and constitutes a part of the Hangay batholith. Previous K–Ar dating gave ages from 336 to 320 Ma (Mongolian Guidebook, 1999) but ages of about 200 Ma were also reported. Zircons from Sample 99-16 were analyzed by SHRIMP and 18 nearly concordant grains defined an age of 229 ± 6 Ma (Fig. 10). This is interpreted as the time of the granite intrusion (for both M99-15 and M99-16). Sample M99-17 came from another small pluton intrusive into Devonian and Carboniferous sediments. It is a hornblende–biotite granodiorite containing diorite enclaves. Its age remains unknown, but we tentatively assign the same age as the Nariyn Teel pluton. Sample M99-18 is a granite of probably Mesozoic age. A biotite analysis defined a biotite-WR isochron age of 119 ± 2 Ma, with I_{Sr} = 0.7077 ± 0.0001. The pluton emplacement age is taken to be 120 Ma.

Ongonites (M99-19, 20, 21). Due to the very high Rb/Sr ratios, the radiogenic in-growth allows a determination of precise intrusive age. The Rb–Sr isotope data of the three WR samples define an isochron age of 118 ± 7 Ma, with I_{Sr} = 0.718 ± 0.042 (MSWD = 0.35; Fig. 11). In addition,

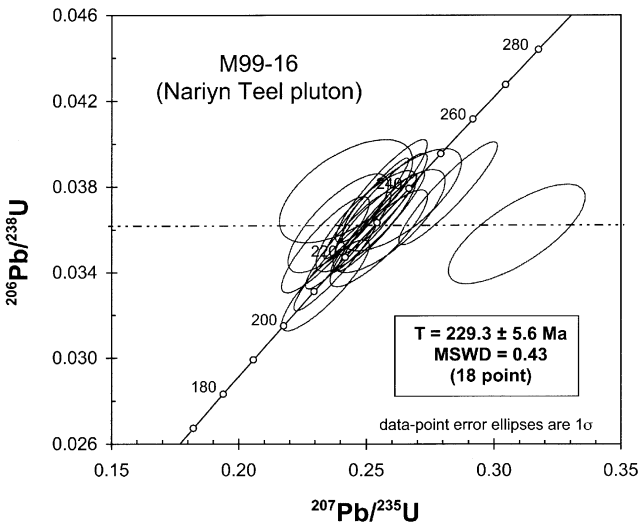

Fig. 10. SHRIMP U–Pb isotope analyses of zircons from a granite of the Nariyn Teel Pluton (M99-16). Eighteen concordant points yield an average $^{206}Pb/^{238}U$ age of 230 ± 6 Ma.

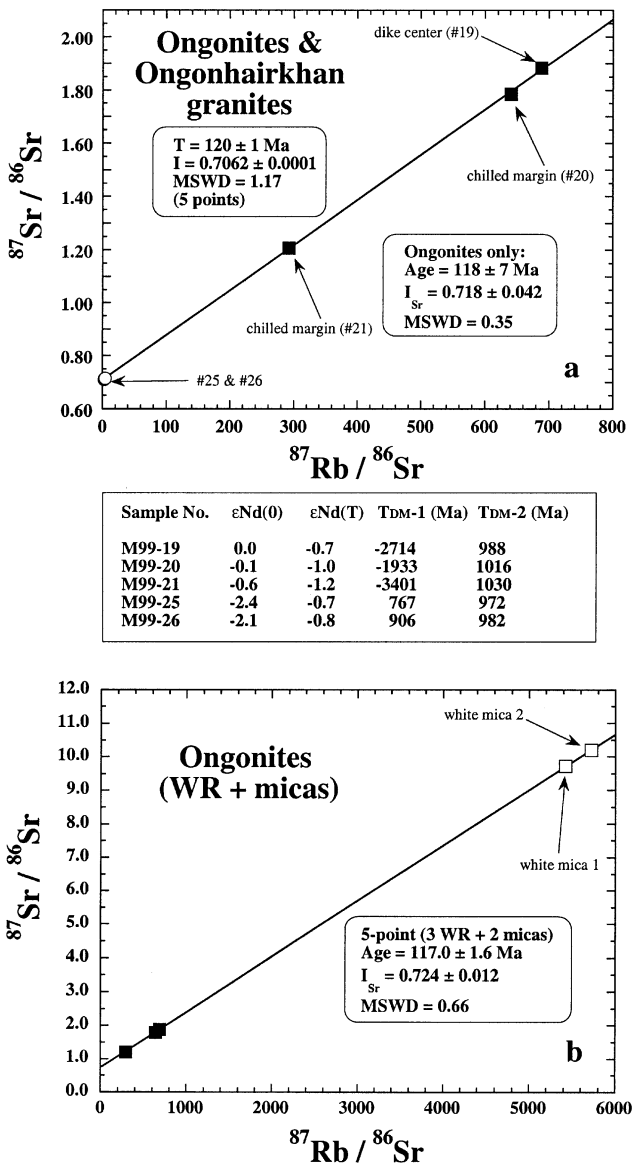

Fig. 11. Rb–Sr isochron diagram for the ongonites and Ongonhairkhan granites. For the ongonites, the age is relatively well constrained, but the initial $^{87}Sr/^{86}Sr$ ratio of ongonites cannot be precisely determined due to the very high Rb/Sr ratios of the rocks. If the Ongonhairkhan granites are combined, a very precise age of 120 ± 1 Ma is obtained with a reasonably well constrained initial ratio of 0.7062 ± 0.0001.

analyses of two white mica separates from sample M99-19 defined a five-point mica-WR isochron of 117 ± 2 Ma, with $I_{Sr} = 0.724 \pm 0.012$. Because the thin dike (2–3 m wide) must have cooled rapidly and because the Rb–Sr isotope blocking temperature of white mica (ca. 500 °C) is similar to the solidus temperature of ongonite magma (ca. 540 °C at 1 kb; Kovalenko et al., 1970), we consider that the age of 118 Ma to represent the time of ongonite dike emplacement. Note that the calculated initial Sr isotope ratio has a very large error, and the high face value of 0.718 or 0.724 should not be taken to infer an S-type granite or used for any petrogenetic discussion. If a very mantle-like initial ratio of 0.704, 0.705 or 0.706 is assumed, a model age of about 120 Ma will still be obtained. On the other hand, the Sm–Nd analysis gave initial $\varepsilon_{Nd}(T)$ values are about zero, clearly indicating a source dominated by the mantle component. Moreover, because of the REE tetrad effect, their Sm/Nd ratios become higher than chondritic, leading to negative one-stage model ages. Using a two-stage model, their model ages are about 1000 Ma, compatible with its relatively juvenile nature.

Ongonhairkhan pluton (M99-25, 26). The pluton was probably emplaced in the same period as the ongonites and formed in an intra-continental environment (Mongolian Guidebook, 1999). A biotite analysis (M99-26) yielded a biotite-WR isochron of 119 ± 2 Ma with $I_{Sr} = 0.7063 \pm 0.0002$. We take 120 Ma for its intrusive age.

Aplite (M99-24). It cuts shaly sediments in the same general area of the Ongonhairkhan pluton and ongonite dikes, but its intrusive age is not constrained. If any value of 0.705–0.715 is assumed to be initial Sr isotopic ratio of the rock, it would have a model age of about 180 Ma. However, the field relationship suggests that the rock was formed contemporaneously with the ongonite dikes and the Ongonhairkhan pluton. We take 120 Ma for its age. This extremely high I_{Sr} value of 0.8944 is not quite geochemically coherent with its $\varepsilon_{Nd}(T)$ at 120 or 180 Ma (−0.8 or −0.2) and T_{DM} of about 1000 Ma, but it can be circumvented by assuming a source with a very high Rb/Sr ratio. A source with Rb/Sr = 15 needs only 300 Ma to increase $^{87}Sr/^{86}Sr$ ratio by 0.192. That is, the aplite can be derived by melting of a 420 Ma-old crustal source with initial $^{87}Sr/^{86}Sr$ ratio of 0.702 to 0.706 and Rb/Sr = 15. This is easily attainable in alkaline or peralkaline granites.

7. Sr–Nd isotopic characteristics

Except ongonites, the initial Sr isotope compositions of the granitoids vary from 0.7042 to 0.7104, with the majority falling about 0.706. Initial ratio is highly sensitive to age correction, and yet our ages are only roughly estimated for most cases. The ongonite age is well determined, but the extremely high Rb/Sr and in-growth radiogenic Sr isotope ratios make it impossible to determine its initial ratio with precision (Jahn et al., 2000a; Wu et al., 2000). Consequently, the calculated I_{Sr} given in Table 2 provide only an indicative value. Broadly, the generally 'low' initial Sr isotope ratios (≤0.707) limit the role of an ancient crustal component in the petrogenesis of the granitoids. In fact, this becomes a common rule for the Phanerozoic granitoids of the whole of Central Asia.

The more rigorous petrogenetic indicator comes from the Nd isotopic compositions. The initial Nd isotope ratios, expressed as $\varepsilon_{Nd}(T)$ values, are insensitive to small error in the intrusive age assignment. We plot the data against assumed emplacement ages (Fig. 12). Literature data for early Precambrian rocks from the Baydrag terrane (Kozakov et al., 1997) are also shown for reference. Our dataset shows that late Paleozoic to Mesozoic rocks (≤250 Ma) have $\varepsilon_{Nd}(T)$ values of 0 to −2 (except M99-17), whereas the Cambro-Ordovician Tsagaan Nuruu granites have the values of −7, the Ulaan Uul red granite of −2.4, and the Nariyn Teel granites of ca. −3. Such near-zero to slightly negative $\varepsilon_{Nd}(T)$ values have also been identified by Kovalenko et al. (1996, 2002) for the rocks intrusive to the Pre-Riphean basement blocks in central Mongolia. Our work confirms their findings. On the other hand, the data of Kovalenko et al. (1996, 2003) show that granitoids emplaced outside of the Precambrian blocks, but still within the 'Caledonian' province, are characterized by positive $\varepsilon_{Nd}(T)$ values. Such a close relationship between Nd isotopic compositions of granitoids and ages (and nature) of the intruded 'basement' rocks is also observed in NE China (Wu et al., 2000, 2003). The lowering of $\varepsilon_{Nd}(T)$ values in the granitic intrusions was evidently effected by the participation of old crustal rocks in their petrogenesis.

8. Discussion

8.1. Comparison with other granitoids from adjacent regions—Inner Mongolia and Transbaikalia

The isotopic characteristics of the Mongolian rocks are quite similar to those observed in granitoids from other parts of the CAOB. We select some Nd isotopic data of granitoids from Inner Mongolia (China) and Transbaikalia (Russia) obtained in Rennes for comparison (Fig. 13). In Inner Mongolia, several periods of granitic intrusions took place in Devonian to Jurassic time. Our samples came from a Paleozoic anorogenic A-type granite suite (280 Ma, Hong et al., 1995, 1996), an arc-related calc–alkaline magmatic belt (Baolidao) composed of gabbroic diorite, quartz diorite, tonalite and granodiorite (SHRIMP zircon age of 309 ± 8 Ma, Chen et al., 2000) and a Mesozoic collision-type granitic suite (Halatu) of mainly monzogranite with subordinate granodiorite and leucogranite (Rb–Sr age of 230 ± 20 Ma, Chen et al., 2000). The Nd isotope data are shown in Fig. 13. The Halatu granites have $\varepsilon_{Nd}(T)$ values of about zero, and their model ages (T_{DM}) of

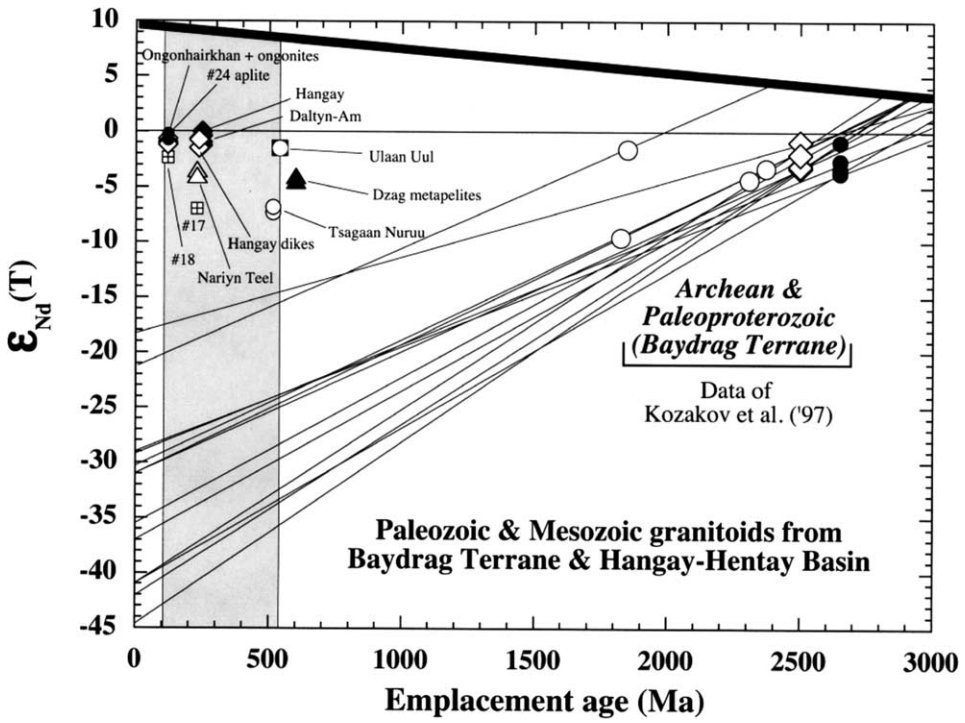

Fig. 12. $\varepsilon_{Nd}(T)$ vs. intrusive age diagram for the studied rocks. The data for Archean and Paleoproterozoic rocks from the Baydrag Terrane are taken from Kozakov et al. (1997) for reference.

800–1200 Ma. The Baolidao gabbro-to-granodiorite suite has 0 to +3 for $\varepsilon_{Nd}(T)$ values and 1100–1500 Ma for model ages. The A-type peralkaline granites have the highest $\varepsilon_{Nd}(T)$ values of +3 to +6 and the youngest model ages of 700–1000 Ma. They are generated by melting of a very juvenile source (>90% mantle component).

The Bryansky Complex of Transbaikalia is a very large intrusive body (ca. 1600 km^2) emplaced in the central part of the Mongolian–Transbaikalian granitoid belt (Litvinovsky et al., 2002). The belt extends for >2000 km and is 200–300 km wide. It comprises about 350 A-type granitic plutons and numerous volcanic fields. U–Pb and Rb–Sr isotopic analyses indicate that the Bryansky Complex was formed at about 280 Ma (Litvinovsky et al., 2002). Both the alkali feldspar and peralkaline suites have very similar initial $^{87}Sr/^{86}Sr$ ratio of 0.705 ± 0.001 as well as $\varepsilon_{Nd}(T)$ values of −2 to −3. On the other hand, the younger Tsagan-Khurtei granitoids (220 Ma) show more positive $\varepsilon_{Nd}(T)$ values (+3) and younger T_{DM} of about 700 Ma.

Fig. 13c presents a $\varepsilon_{Nd}(T)$ vs. model age plot with two reference fields (Hercynian and Himalayan granites). The Central Asian data are clearly distinguished from the European Hercynian and Caledonian granites, and even more from the leucogranites of the Himalayas (Jahn et al., 2000a,b).

The granitoids of the northern belt of the CAOB, from central-northern Mongolia to Transbaikalia, have been extensively studied by Kovalenko et al. (1992, 1996, 2003). These authors delineated three isotope provinces ('Caledonian', 'Hercynian', and 'pre-Riphean') which coincide with three tectonic zones of corresponding age for the northern belt of the CAOB. Without exceptions, Phanerozoic granites emplaced into 'Caledonian' and 'Hercynian' tectonic zones have positive $\varepsilon_{Nd}(T)$ values, suggesting their juvenile characteristics; whereas those intruded into the pre-Riphean basement show variable $\varepsilon_{Nd}(T)$ from positive to negative values, indicating variable contributions of old Precambrian crust in the generation of the granitic rocks.

8.2. Estimate of the proportions of juvenile crust

The proportions of juvenile crust in any given area in the CAOB must be evaluated from detailed knowledge about the distribution of lithological types, of which the granitoids must be further estimated using the isotope tracer technique. This is not an easy task. However, for individual granitoid bodies, this can be done reasonably well using a two-component mixing calculation. Assuming a fixed depleted mantle component and variable crustal end-members, the result of the calculation is shown in Fig. 14. The proportion of the mantle component (or %juvenile crust) for positive $\varepsilon_{Nd}(T)$ granites varies from 60 to 100% depending on the compositions of the assumed crustal end-members. For the Mongolian granitoids we assume $\varepsilon^m_{Nd} = +8$ and $[Nd]^m = 15$ ppm for the juvenile (basaltic) component, and $\varepsilon^c_{Nd} = -30$ and $[Nd]^c = 25$ ppm for the crustal component (= the Baidarik Block, Fig. 12

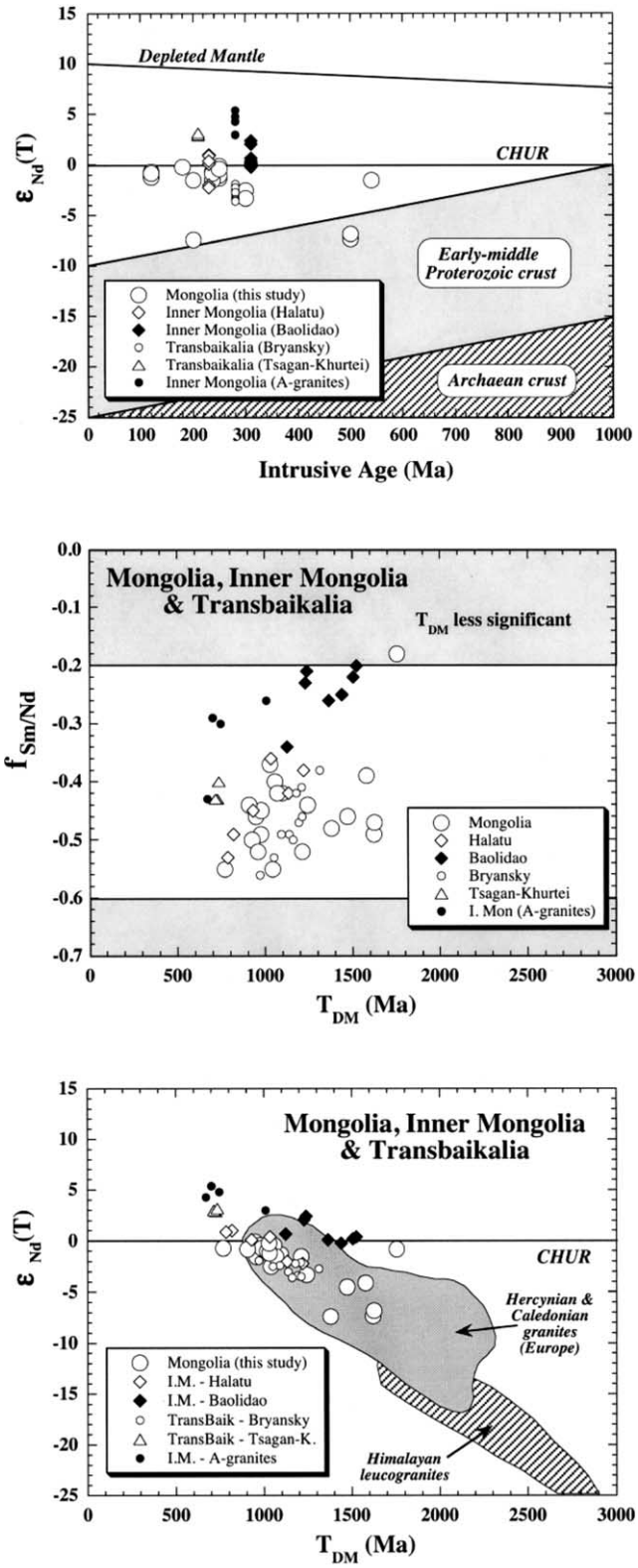

Fig. 13. Isotope diagrams for granitoids from Mongolia, Inner Mongolia, Transbaikalia. (a) $\varepsilon_{Nd}(T)$ vs. intrusive ages, (b) $f_{Sm/Nd}$ vs. T_{DM} (one stage), and (c) $\varepsilon_{Nd}(T)$ vs. T_{DM} (one stage). Data source for Inner Mongolia: Chen et al. (2000), Jahn, unpublished; for Transbaikalia: Litvinovsky et al. (2002). The fields for Hercynian and Caledonian granites and Himalayan leucogranites, from the compilation of Jahn et al. (2000).

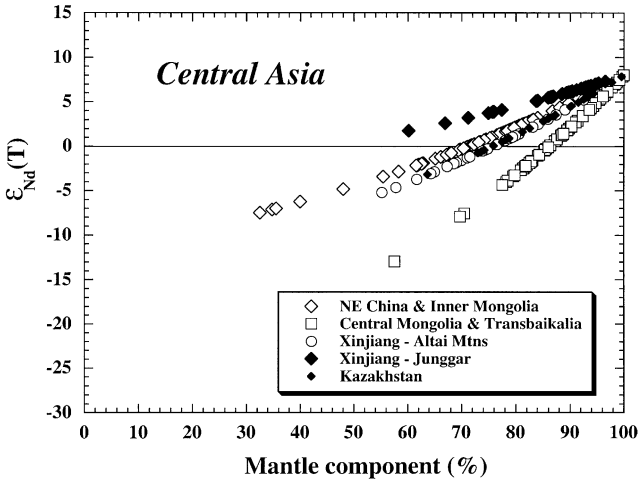

Fig. 14. Estimate of proportions of the mantle or juvenile component in the generation of Central Asian granitoids. The equation used is: $X^m = (\varepsilon^c - \varepsilon^r)Nd_c/[\varepsilon^r(Nd_m - Nd_c) - (\varepsilon^m Nd_m - \varepsilon_c Nd_c)]$, where X^m = % mantle component (represented by basalt). ε^c, ε^r, ε^m = Nd isotope compositions of the crustal component, rock measured, and mantle component, respectively. Nd_c, Nd_m = Nd concentrations in the crustal and mantle components, respectively. Parameters used: $\varepsilon^m = +8$, $\varepsilon^c = -12$ (NE China), -30 (Central Mongolia), -15 (Altai and Kazakhstan), -4 (Junggar), -18 (Tianshan). $Nd_m = 15$ ppm, $Nd_c = 25$ ppm.

or Kozakov et al., 1997). The result of mass balance calculation (Fig. 14) indicates that the juvenile component would represent $\geq 80\%$ for $\varepsilon_{Nd}(T)$ values of -5, and ca. 85% if the values are close to zero. If a Bumburger gneiss of 70 ppm of Nd (Kozakov et al., 1997) is used, the proportion of crustal contribution would be further reduced. If a Meso- or Neoproterozoic rock is assumed to be the crustal component, the percentage of the mantle component would be diminished. In this connection, the Tsagaan Nuruu granites could have been derived by remelting of a Meso- to Neoproterozoic rocks, or a younger source mixed with a larger proportion of the Baydrag cratonic component. On the other hand, some negative $\varepsilon_{Nd}(T)$ values for the granites from the Hangay terrane could be interpreted in two ways: (1) their ultimate source was a long-term enriched mantle, or (2) presence of Precambrian rocks under the Hangay Basin, which have participated in the generation of the late Paleozoic granitoids.

The general scenario in Central Asia as shown in Fig. 14 implies extensive mantle differentiation and rapid crustal growth during the Phanerozoic. The massive juvenile granitoids were considered to be generated in two processes: (1) subduction zone magmatism, related to the successive building of island arcs, and (2) basaltic underplating, operated after accretion of island arc complexes and during post-accretionary extensional phase. Thus, new crust was formed by both lateral accretion of island arcs and vertical accretion of underplated basaltic magmas and their derivatives. A more detailed discussion is presented by Jahn (2003).

9. Conclusions

The present survey-type study leads to the following conclusions:

1. Major element analyses indicate that, except for a diorite and a granodiorite, all the granitoids are slightly peraluminous and can be classified as granites s.s. (including monzogranite, syenogranite and alkali feldspar granite) based on the Q' vs. ANOR scheme (Streckeisen and Le Maitre, 1979). All belong to the high-K calc–alkaline series in a K_2O vs. SiO_2 plot.
2. SHRIMP zircon analyses yield new age information: 514 ± 10 Ma for the intrusion of the Tsagaan Nuruu stock, and 230 ± 6 Ma for the emplacement of the Nariyn Teel pluton.
3. Four biotite analyses provided minimum ages for the Daltyn-Am stock (>242 Ma), the Hangay batholith (>234 Ma), un unnamed pluton, M99-18 (120 Ma), and the Ongonhairkhan pluton (120 Ma).
4. Three ongonite samples and two Ongonhairkhan granites define a whole-rock Rb–Sr isochron age of 120 ± 1 Ma. Two additional white mica analyses confirmed the age assignment. Geochemically, the ongonites possess tetrad REE patterns and show many trace element features of non-CHARAC behavior. This is attributed to intense interaction between a hydrothermal fluid and a highly differentiated late-stage magmatic liquid.
5. The Dzag metapelites have trace element abundances very similar to average post-Archean shales. They represent a well-mixed and homogenized sample, probably derived from a large area covering Proterozoic and Archean terranes that existed before the formation of the Paleozoic island arcs.
6. Initial $^{87}Sr/^{86}Sr$ ratios for most granitoids are about 0.706, and $\varepsilon_{Nd}(T)$ values range from 0 to −3 except for the Cambro-Ordovician Tsagaan Nuruu granites (−7). These isotopic compositions limit the participation of old Precambrian crustal rocks in the generation of the Phanerozoic granitoids.
7. The isotope scenarios of the granitoids from Central Mongolia and adjacent Inner Mongolia and Transbaikalia are quite similar, and are also typical of the entire Central Asian Orogenic Belt. The early Precambrian Baydrag cratonic rocks have participated in the generation of the Tsagaan Nuruu granites.

Acknowledgements

The chemical compositions were determined using ICP-AES and ICP-MS by the staff of the Analytical Center at CRPG-Nancy. Rb–Sr and Sm–Nd isotopic analyses were performed by Nicole Morin and Joël Macé at Rennes. We deeply appreciate the assistance of the above laboratory staff. V.I. Kovalenko and Brian Windley reviewed the manuscript and provided very useful comments and suggestions. This work represents a contribution to the International IGCP Programme, project IGCP-420 (Crustal Growth in the Phanerozoic: Evidence from East-Central Asia). Our field work in Mongolia (BmJ and RC) was supported by the French IGCP Committee.

References

Antipin, V.S., Savina, E.A., Mitichkin, M.A., Perelyaev, V.I., 1999. Rare-metal lithium–fluorine granites, ongonites, and topazites of the southern Baikal region. Petrology 7, 147–159.

Badarch, G., Cunningham, W.D., Windley, B.F., 2002. A new terrane subdivision for Mongolia: implications for the Phanerozoic crustal growth of Central Asia. Journal of Asian Earth Sciences 21, 87–110.

Bau, M., 1996. Controls on the fractionation of isovalent trace elements in magmatic and aqueous system: evidence from Y/Ho, Zr/Hf, and lanthanide tetrad effect. Contributions to Mineralogy and Petrology 123, 323–333.

Buchan, A.C., Cunningham, W.D., Windley, B.F., Tomorhuu, D., Dorjnaamjaa, D., 1999. The Bayankhongor ophiolite zone, central Mongolia: a suture in the Altaids. In: Badarch, G., Jahn, B.M. (Eds.), IGCP-420 Second Workshop Abstract and Excursion Guidebook, Géosciences Rennes, Hors série No. 2, pp. 8–10.

Buchan, C., Cunningham, W.D., Windley, B.F., Tomurhuu, D., 2001. Structural and lithological characteristics of the Bayankhongor ophiolite zone, Central Mongolia. Journal of the Geological Society, London 158, 445–460.

Buchan, C., Pfander, J., Kroner, A., Brewer, T.S., Tomurtogoo, O., Tomurhuu, D., Cunningham, D., Windley, B., 2002. Timing of accretion and collisional deformation in the Central Asian orogenic Belt: implications of granite geochronology in the Bayankhongor Ophiolite Zone. Chemical Geology 192, 23–45.

Budnikov, S.V., Kovalenko, V.I., Kotov, A.B., Salnikova, E.B., Kovach, V.P., 1999. The ages and sources of the Hangay batholith (Central Mongolia). In: Badarch, G., Jahn, B.M. (Eds.), IGCP-420 Second Workshop Abstract and Excursion Guidebook, Géosciences Rennes, Hors série No. 2, p. 11.

Chen, B., Jahn, B.M., 2003. Genesis of post-collisional granitoids and basement nature of the Junggar Terrane, NW China: Nd–Sr isotope and trace element evidence. Journal of Asian Earth Sciences.

Chen, B., Jahn, B.M., Wilde, S., Xu, B., 2000. Two contrasting Paleozoic magmatic belts in northern Inner Mongolia, China: petrogenesis and tectonic implications. Tectonophysics 328, 157–182.

Condie, K.C., 1993. Chemical composition and evolution of the upper continental crust: contrasting results from surface samples and shales. Chemical Geology 104, 1–37.

Gordienko, I.V., 1987. Paleozoic Magmatism and Geodynamics of Central-Asian Foldbelt, Nauka, Moscow, p. 238.

Hong, D.W., Huang, H.Z., Xiao, Y.J., Xu, H.M., Jin, M.Y., 1995. Permian alkaline granites in central Inner Mongolia and their geodynamic significance. Acta Geologica Sinica 8, 27–39.

Hong, D.W., Wang, S.G., Han, B.F., Jin, M.Y., 1996. Post-orogenic alkaline granites from China and comparisons with anorogenic alkaline granites elsewhere. Journal of SE Asian Earth Sciences 13, 13–27.

Irber, W., 1999. The lanthanide tetrad effect and its correlation with K/Rb, Eu/Eu*, Sr/Eu, Y/Ho, and Zr/Hf of evolving peraluminous granite suites. Geochimica Cosmochimica Acta 63, 489–508.

Jahn, B.M., 2003. The Central Asian Orogenic Belt and growth of the continental crust in the Phanerozoic. Geological Society of London Special Publications. Accepted for publication.

Jahn, B.M., Cornichet, J., Cong, B.L., Yui, T.F., 1996. Ultrahigh-εNd eclogites from an ultrahigh-pressure metamorphic terrane of China. Chemical Geology 127, 61–79.

Jahn, B.M., Wu, F.Y., Lo, C.H., Tsai, C.H., 1999. Crust-mantle interaction induced by deep subduction of the continental crust: geochemical and Sr–Nd isotopic evidence from post-collisional mafic-ultramafic intrusions of the northern Dabie complex, central China. Chemical Geology 157, 119–146.

Jahn, B.M., Wu, F.Y., Chen, B., 2000a. Granitoids of the Central Asian Orogenic Belt and continental growth in the Phanerozoic. Transactions Royal Society of Edinburgh: Earth Sciences 91, 181–193.

Jahn, B.M., Wu, F.Y., Chen, B., 2000b. Massive granitoid generation in Central Asia: Nd isotope evidence and implication for continental growth in the Phanerozoic. Episodes 23, 82–92.

Jahn, B.M., Wu, F.Y., Capdevila, R., Martineau, F., Zhao, Z.H., Wang, Y.X., 2001. Highly evolved juvenile granites with tetrad REE patterns: the Woduhe and Baerzhe granites from the Great Xing'an Mountain in NE China. Lithos 59, 171–198.

Kepezhinskas, P.K., Kepezhinskas, K.B., Puchtel, I.S., 1991. Lower Paleozoic oceanic crust in Mongolian Caledonides: Sm–Nd isotope and trace element data. Geophysical Research Letters 18, 1301–1304.

Keto, L.S., Jacobsen, S.B., 1987. Nd and Sr isotopic variations of Early Paleozoic oceans. Earth and Planetary Science Letters 84, 27–41.

Kotov, A.B., Kozakov, I.K., Bibikova, E.V., Sal'nikova, E.B., Kirnozova, T.I., Kovach, V.P., 1995. Duration of regional metamorphic episodes in areas of polycyclic endogenic processes: a U–Pb geochronological study. Petrology 3, 621–630.

Kovalenko, N.I., Kuzmin, M.I., Ceden, C., Vladykin, N.V., 1969. Lithium-fluorine quartz keratophyre (ongonite), a new variety of sub-volcanic magmatic dikes. Ezhegodnik 1969, Siberian Institute of Geochemistry, Irkutzk, (pp. 85–99; in Russian).

Kovalenko, V.I., Tsareva, G.M., Yarmolyuk, V.V., Troisky, V.A., Farmer, G.L., Chernishev, I.V., 1992. Sr–Nd isotopic compositions and the age of rare-metal peralkaline granitoids from western Mongolia. Dokladi Akademiia Nauk 237, 570–574 (in Russian).

Kovalenko, V.I., Yarmolyuk, V., Bogatikov, O., 1995. Magmatism, geodynamics, and metallogeny of Central Asia, Miko Commercial Herald Publishers, Moscow, 272 pp.

Kovalenko, V.I., Yarmolyuk, V.V., Kovach, V.P., Kotov, A.B., Kozakov, I.K., Sal'nikova, E.B., 1996. Sources of Phanerozoic granitoids in Central Asia: Sm–Nd isotope data. Geochemistry International 34, 628–640.

Kovalenko, V.I., Yarmolyuk, V.V., Kovach, V.P., Kotov, A.B., Kozakov, I.K., Salnikova, E.B., Larin, A.M., 2003. Isotope provinces, mechanisms of generation and sources of the continental crust in the Central Asian Mobile Belt: geological and isotopic evidence. Journal of Asian Earth Sciences in press.

Kozakov, I.K., Kotov, A.B., Kovach, V.P., Sal'nikova, E.B., 1997. Crustal growth in the geological evolution of the Baidarik block, central Mongolia: evidence from Sm–Nd isotopic systematics. Petrology 5 (3), 201–207.(Translated from Petrologiya 5 227–235).

Kozakov, I.K., Kotov, A.B., Salnikova, E.B., Kovach, V.P., Nutman, A., Bibikova, E.V., Kirnozova, T.I., Todt, W., Kröner, A., Yakovleva, S.Z., Lebedev, V.I., Sugorakova, A.M., 2001. Timing of the structural evolution of metamorphic rocks in the Tuva-Mongolian Massif. Geotectonics 35, 165–184.

Kurimoto, C., Tungalag, F., 1998. K–Ar ages of white micas from pelitic schists of the Bayankhongor area, west Mongolia. Bulletin of Geological Survey of Japan 49, 19–23.

Litvinovsky, B.A., Zanvilevich, A.N., Wickham, S.M., 1994. Angara-Vitim batholith, transbaikalia: structure, petrology and petrogenesis. Russian Geology and Geophysics 35, 190–203.

Litvinovsky, B.A., Jahn, B.M., Zanvilevich, A.N., Saunders, A., Poulain, S., Kuzmin, D.V., Reichow, M.K., Titov, A.V., 2002. Petrogenesis of syenite-granite suites from the Bryansky complex (Transbaikalia Russia): implications for the origin of A-type granitoid magmas. Chemical Geology 189, 105–133.

Liu, W., 1990. Ages and petrogenesis of granitoids in the Altai Mountains, Xinjiang, China. Geotectonica and Metallogenica 14, 43–56 (in Chinese, with English abstract).

Ludwig, K.R., 1999. ISOPLOT/Ex. Version 2.06. A geochronological toolkit for Microsoft Excel. Berkeley Geochronology Center Special Publications No. 1a, 49 pp.

Maniar, P.D., Piccoli, P.M., 1989. Tectonic discrimination of granitoids. Geological Society of America Bulletin 101, 635–643.

Masuda, A., Akagi, T., 1990. Lanthanide tetrad effect observed in leucogranites from China. Geochemical Journal 23, 245–253.

Masuda, A., Nakamura, N., Tanaka, T., 1973. Fine structures of mutually normalized rare-earth patterns of chondrites. Geochimica Cosmochimica Acta 37, 239–248.

McLennan, S.M., 2001. Relationships between the trace element composition of sedimentary rocks and upper continental crust. G3 (Geochem–Geophys–Geosys), 2000GC000109.

Mitrofanov, F.P., Bibikova, E.V., Gracheva, T.V., Kozakov, I.K., Sumin, L.V., Shuleshko, I.K., 1985. Archaean isotope age of tonalite (grey) gneisses in Caledonian structure of Central Mongolia. Doklady Academii Nauk SSSR 284 (3), 671–674 (in Russian).

Mongolian Guidebook, 1999. In: Badarch, G., Jahn, B.M. (Eds.), IGCP-420 Second Workshop Abstract and Excursion Guidebook, Géosciences Rennes, Hors série No. 2, 93 pp (Abstracts) and 85 pp (Guidebook).

Oyungerel, S., Takahashi, Y., 1999. New radiometric age data of the granitoids in Bayankhongor area, Central Mongolia. Mongolian Geoscientist 13, 38–40.

Parfenov, L.M., Popeko, L.I., Tomurtogoo, O., 1999. The problems of tectonics of the Mongol–Okhotsk orogenic belt. Pacific Oceanic Geology 18, 24–43.

Rikhter, A.V., Dergunov, A.B., Lunova, O.I., Ryazantsev, A.V., 1994. Granite-metamorphic complex in the cover of the Bumburger Massif (Mongolia). Geotektonika 4, 73–79.

Ruzhentsev, S.V., Mossakovskiy, A.A., 1996. Geodynamics and tectonic evolution of the Central Asian Paleozoic structures as the result of the interaction between the Pacific and Indo-Atlantic segments of the earth. Geotectonics 29, 211–311.

Sengör, A.M.C., Natal'in, B.A., 1996. Turkin-type orogeny and its role in the making of the continental crust. Annual Review of Earth and Planetary Sciences 24, 263–337.

Sengör, A.M.C., Natal'in, B.A., Burtman, V.S., 1993. Evolution of the Altaid tectonic collage and Paleozoic crustal growth in Eurasia. Nature 364, 299–307.

Stemprok, M., 1991. Ongonite from ongon khairkhan, Mongolia. Mineralogy and Petrology 43, 255–273.

Streckeisen, A., Le Maitre, R.W., 1979. A chemical approximation to the modal QAPF classification of the igneous rocks: N. Jb. Miner. Abh. 136, 169–206.

Sun, S.S., McDonough, W.F., 1989. Chemical and isotopic systematics of oceanic basalts: implications for mantle composition and processes. In: Saunders, A.D., Norry, M.J. (Eds.), Magmatism in Ocean Basins, Geological Society of London Special Publications, vol. 42., pp. 313–345.

Takahashi, Y., Arakawa, Y., Oyungerel, S., Naito, K., 2000. Geochronological data of granitoids in the Bayankhongor area, central Mongolia. Bulletin of Geological Society of Japan 51, 167–174.

Taylor, S.R., McLennan, S.M., 1985. The continental crust: its composition and evolution, Blackwell, Oxford, 312 pp.

Taylor, S.R., McLennan, S.M., 1995. The geochemical evolution of the continental crust. Review of Geophysics 33, 241–265.

Teraoka, Y., Suzuki, M., Tungalag, F., Ichinnorov, N., Sakamaki, Y., 1996. Tectonic framework of the Bayanhongor area, west Mongolia. Bulletin of Geological Society of Japan 47, 447–455.

Vladimirov, A.G., Ponomareva, A.P., Shokalskii, S.P., Khalilov, V.A., Kostitsyn, Yu.A., Ponomarchuk, V.A., Rudnev, S.N., Vystavnoi, S.A., Kruk, N.N., Titov, A.V., 1997. Late Paleozoic–early Mesozoic granitoid magmatism in Altai. Russian Geology and Geophysics 38, 755–770.

Wickham, S.M., Litvinovsky, B.A., Zanvilevich, A.N., Bindeman, I.N., 1995. Geochemical evolution of Phanerozoic magmatism in Transbaikalia, East Asia: a key constraint on the origin of K-rich silicic magmas

and the process of cratonization. Journal of Geophysical Research 100, 15641–15654.

Wickham, S.M., Alberts, A.D., Zanvilevich, A.N., Litvinovsky, B.A., Bindeman, I.N., Schuble, E.A., 1996. A stable isotope study of anorogenic magmatism in East Central Asia. Journal of Petrology 37, 1063–1095.

Williams, I.S., 1998. U–Th–Pb geochronology by ion microprobe. In: McKibben, M.A., Shanks, W.C., Ridley, W.I. (Eds.), Applications of microanalytical techniques to understanding mineralizing processes, Review of Economic Geology, vol. 7., pp. 1–35.

Wu, F.Y., Jahn, B.M., Wilde, S., Sun, D.Y., 2000. Phanerozoic crustal growth: Sr–Nd isotopic evidence from the granites in northeastern China. Tectonophysics 328, 89–113.

Wu, F.Y., Sun, D.Y., Li, H.M., Jahn, B.M., Wilde, S., 2002. A-type granites in Northeastern China: age and geochemical constraints on their petrogenesis. Chemical Geology 187, 143–173.

Wu, F.Y., Jahn, B.M., Wilde, S., Lo, C.H., Yui, T.F., Lin, Q., Ge, W.C., Sun, D.Y., 2003. Highly fractionated I-type granites in NE China (II): isotopic geochemistry and implications for crustal growth in the Phanerozoic. Lithos 67, 191–204.

Zanvilevich, A.N., Litvinovsky, B.A., Wickham, S.M., 1995. Genesis of alkaline and peralkaline syenite-granite series: the Kharitonovo pluton (Transbaikalia, Russia). Journal of Geology 103, 127–145.

Zonenshain, L.P., Kuzmin, M.I., Natapov, L.M., 1990. Geology of the USSR: A Plate Tectonic Synthesis, AGU Geodynamics Series, vol. 242., 242 pp.

Zorin, Yu.A., 1999. Geodynamics of the western part of the Mongolia-Okhotsk collisional belt, Transbaikal region (Russia) and Mongolia. Tectonophysics 306, 33–56.

Zou, T.R., Cao, H.Z., Wu, B.Q., 1988. Discrimination of orogenic and anorogenic granites in Altai, Xinjiang. Acta Geologica Sinica 3, 228–243 (in Chinese with English abstract).